Tectonic controls on magmatic tempo in an active continental margin: Insights from the Early Cretaceous syn-tectonic magmatism in the Changle-Nan'ao Belt, South China

Wei Wei, Wei Lin, Yan Chen, Michel Faure, Wenbin Ji, Quanlin Hou, Quanren Yan, Qingchen Wang

Tectonic controls on magmatic tempo in an active continental margin: insights from the Early Cretaceous syn-tectonic magmatism in the Changle-Nan'ao Belt, South China

Wei Wei[1,2,3,4], Wei Lin[1,2]*, Yan Chen[3], Michel Faure[3], Wenbin Ji[1,2,3,5], Quanlin Hou[2], Quanren Yan[2], Qingchen Wang[1]

1 SKL, Institute of Geology and Geophysics, Chinese Academy of Sciences, Beijing 100029, China

2 College of Earth and Planetary Sciences, University of Chinese Academy of Sciences, Beijing 100049, China

3 Université d'Orléans, CNRS, BRGM, ISTO, UMR 7327, 45071 Orléans, France

4 Shanghai Sheshan National Geophysical Observatory, Shanghai 200062, China

5 Department of Geology, Northwest University, Xi'an 710069, China

* linwei@mail.iggcas.ac.cn

Key points

▸The 130-105 Ma syn-tectonic plutons intruded the Changle-Nan'ao Belt in a NW-SE shortening regime caused by a microcontinent collision.

▸The shortening/extension regimes were coeval with magmatic lull/flare-up in the East Asia Continental Margin during the Cretaceous.

▸The collision causing break-off can account for the plutonism in the Changle-Nan'ao Belt during the magmatic lull of the South China Block.

This article has been accepted for publication and undergone full peer review but has not been through the copyediting, typesetting, pagination and proofreading process, which may lead to differences between this version and the Version of Record. Please cite this article as doi: 10.1029/2022JB025973.

Abstract:

The cause of magmatic tempo in an active plate margin remains controversial, partly due to lack of structural analysis. During 130-105 Ma, the magmatism in the South China Block (SCB) was significantly reduced (lull) and restricted around the Changle-Nan'ao Belt (CNB) while the magmatism was highly active (flare-up) in North China. For unveiling the tectonic role on magmatism, a multidisciplinary study including field and microscopic structural observations, magnetic fabric measurement (AMS), and zircon/monazite dating was conducted on the plutons with oriented minerals in the CNB. Structural analysis and AMS results show a highly clustered NE-striking vertical foliation developed during the emplacement indicating a syn-emplacement NW-SE shortening regime. The geochronology results confirm that the emplacement occurred during 130-105 Ma. Regional geologic correlation indicates that the collision between the Dangerous Grounds-West Philippines Block and SCB was responsible for this shortening regime. The collected depleted zircon ε Hf(t) data suggest that a possible collision-triggered slab break-off caused the syn-collisional magmatic activity around the CNB. This study shows that the magmatic lull in the SCB was coeval with a crustal shortening regime due to the arrival of a microcontinent carried by the subduction slab, while the magmatic flare-up was coeval with an extensional regime due to the subduction roll-back and retreat as evidenced by the Cretaceous evolution of the SCB before and after the collision and that of North China which is unaffected by the collision. The cause of magmatic tempo in the continental margin is largely due to the tectonic evolution of underlain subduction slabs.

Plain Language Summary

Magmatic activity is closely connected to human life as it provides us with useful metals, releases greenhouse gases, triggers natural hazards. It is necessary to explore what controls a magmatic activity. Several previous studies considered that a shortening regime with thickened crust causes strong magmatism (flare-up). The South China Block (SCB) featured by alternating magmatic flare-up and lulls, provides an

appropriate research target to test this hypothesis. During the Cretaceous, the SCB was dominated by an extensional regime caused by the Paleo-Pacific oceanic slab subduction. However, our structural analyses on the SCB document a shortening regime caused by the collision between the SCB and a microcontinent carried by the Paleo-Pacific oceanic slab in the period of the Cretaceous. During the collision, the SCB was generally featured by a magmatic lull, although magmatic activity was only observed around the Changle-Nan'ao Belt, probably caused by the break-off of the subducted Paleo-Pacific oceanic slab. Before and after the collision, the extensional regime caused by Paleo-Pacific oceanic slab subduction was coeval with magmatic flare-up. This study questions the previous claims and proposes that the tectonic evolution of the subducting slab may control the magmatic flare-up and lull in the overlain active continental margin.

Keywords:

AMS of syn-tectonic pluton, magmatic flare-up and lull, East Asia Continental Margin, South China Block, Dangerous Grounds-West Philippines Block, Changle-Nan'ao Belt

1. Introduction

The arc magmatism in the convergent plate margin plays an important role in the plate tectonic evolution, the continental growth and even the Earth chemical differentiation (Paterson & Ducea, 2015). Statistics on the convergent plate margins distributed worldwide indicates that there are significant periodic variations of magmatism intensity (magmatic tempo), in which high and low volume magmatic events are referred to as magmatic flare-up and lull, respectively (Armstrong, 1988; Ducea et al., 2015; Zhang et al., 2019). The cause of magmatic tempo has long been debated and remained inconclusive partly due to a lack of structural analysis (Paterson & Ducea, 2015). In this regard, previous research provided diversified arguments on the roles of subducting slab in magmatic activity. Some studies take into account the

variation of the plate convergence rate, and subduction retreating/advancing (e.g., Huang & Lundstrom, 2007; Shellnutt et al., 2014; Zhang et al., 2019), while others tend to consider that the magmatic flare-up is rather related to crustal shortening events in the active continental margin where fold and thrust belts lead to a thickened crust (Ducea & Barton, 2007; Ducea et al., 2015; Paterson & Ducea, 2015).

As an active continental margin during the Late Mesozoic, the East Asia Continental Margin (EACM) was significantly affected by the Paleo-Pacific slab subduction, and also featured by alternations of magmatic flare-ups and lulls (Figures 1a, 1b and 1c; Li & Li, 2007; Li, Zhang et al., 2014; Lin & Wei, 2018; Wu et al., 2019; Lin et al., 2021). The widely distributed Late Mesozoic structures, such as crustal-scale faulting system, make the EACM a favorable target to conduct an analysis on the relationship between the tectonics and magmatic tempo. In the long evolution of the EACM during the Late Mesozoic, the Cretaceous was an important period, during which the magmatism in the South China Block (SCB; the southern part of the EACM) shows a coastal-ward migration trend (Li & Li, 2007), and is featured by a 140-130 Ma flare-up, a 130-105 Ma lull and a 105-80 Ma flare-up (Figures 1a, 1c and 2a; Jiang et al., 2015). In the 130-105 Ma lull period, the magmatic activity was restricted around the narrow Changle-Nan'ao Belt (CNB; Figure 2). While in the northern part of the EACM, the magmatism was active in the North China Craton (NCC), Korean Peninsular and Japanese Islands, and it also shows a coastal-ward migration trend with a 130-120 Ma magmatic flare-up in the NCC (Sagong et al., 2005; Wu et al., 2007; Lin et al., 2021). Thus, in the same coastward migration setting in both the South China Block and North China Craton during the Early Cretaceous (K_1), however, a 130-105 Ma lull developed in the SCB while the flare-up continued in the NCC.

As the Paleo-Pacific Slab has entirely subducted, its subduction history can only be traced by its footprints recorded in the EACM. Located at the southeastern-most part of the EACM, the Changle-Nan'ao Belt (CNB) is one of most suitable study targets for reconstructing the Early Cretaceous (K_1) tectonic evolution of the Paleo-Pacific slab subduction for the following two reasons: first, it is the nearest to the subduction zone, and can thus provide direct constraints on the plate boundary activity; second, there are

developed continuous plutonism during the Early Cretaceous (K_1), while the plutonism is lacking elsewhere in the SCB owing to the 130-105 Ma magmatic lull.

In this study, in order to clarify the cause of the Cretaceous magmatic lull in the SCB and further explore the potential controls on general magmatic tempo, a multidisciplinary approach, including AMS, field and microscopic observations, zircon LA-ICPMS and monazite EPMA chemical dating, has been conducted on the K_1 syn-tectonic plutons in the CNB. Together with regional geologic correlation, and Hf isotope statistics in the CNB and its adjacent areas, three questions are intended to be addressed: 1) What was the tectonic evolution of the CNB and SCB during the K_1? 2) What was the geodynamic background of the K_1 tectonics of SCB? 3) How can the magmatism be linked to the tectonic and geodynamic contexts?

2. Geological setting

2.1. The South China Block and its adjacent blocks

Located in the EACM, the SCB is a continental block formed in the Neoproterozoic (e.g., Charvet et al., 1996; Shu et al., 2021). It collided with the NCC located to its north during the Paleozoic along the Qinling-Dabie orogen (e.g., Mattauer et al., 1985), and merged with the Indochina Block located to its south during the Early Triassic along the Indochina orogen (e.g., Faure et al., 2014). During the Mesozoic, a 1300 km wide NW-directed fold-and-thrust belt was formed in the Triassic, which was interpreted as the result of the Paleo-Pacific slab subduction while its roll-back in the Cretaceous may account for the large extension in the SCB (Li & Li, 2007; Li, Zhang et al., 2014). Marine investigations revealed a widespread Cretaceous magmatism extending from the SE coastal area of the SCB, the northern part of the South China Sea, to South Vietnam, forming a huge magmatic belt in the EACM (Figure 1a; Fyhn et al., 2010; Morley, 2012; Hennig-Breitfeld et al., 2021).

The Dangerous Grounds-West Philippines Block (DGWP) is a continental block separated by the Oligocene opening of the South China Sea from the SCB to its north (Figure 1a; Faure et al., 1989; Fyhn et al., 2010; Hall, 2012). It collided with the East

Philippine Mobile Zone to its east and the Borneo Continental Block to its south during the Miocene (Hall, 2013; Yumul et al., 2009). The origin of this block is still in dispute, either an Asian origin, or as a former part of Sundaland (Hutchison & Vijayan, 2010; Zhou et al., 2008; Hall, 2012). The paleogeographic location of this block in the Paleo-Pacific Ocean during the Mesozoic was uncertain (Hall, 2012). In the West Philippines Islands, ophiolites crop out in several places. In the NE end of the DGWP, the Early Cretaceous ophiolites outcropped in the Mindoro Island (Figure 1d; Yumul et al., 2007) and were involved in a S-directed thrust. These ophiolites were interpreted as a part of the vanished ocean located between the DGWP and SCB (Faure et al., 1989). To the north of this suture zone, the Permian granite in the Mindoro Island was correlated to those Permian granites in the SCB (Figures 1a and 1d; Knittel et al., 2010). The Oligocene ophiolites in the Mindoro Island were considered as the suture zone between the DGWP and East Philippine Mobile Zone (Yumul et al., 2009). The Late Cretaceous to Eocene ophiolites in the South Palawan Island were interpreted as the suture zone between the DGWP and Borneo (Figure 1a; Hall, 2013). The boundary between the DGWP and Sunda Shelf is underneath the South China Sea, however, this boundary continued to the Lupar line in inland of Borneo (Figure 1a; Fyhn et al., 2010).

2.2. Litho-tectonic units of the Changle-Nan'ao Belt

The Changle-Nan'ao Belt (CNB) is a NE-SW striking ca. 400 km long and 40-60 km wide ductile shear zone located at the southeast coast of the SCB (Figures 1a and 2a; Cui et al., 2013; Wei et al., 2015). On the basis of lithology and structure, the CNB can be divided into five litho-tectonic units (Figure 2a), namely (1) the pervasively deformed gneiss unit, located in the SE part of CNB, consisting of migmatite, orthogneiss and micaschist with amphibolite or granulite metamorphic facies (Chen, 1997; Cui et al., 2013; Liu et al., 2012; Tong & Tobisch, 1996); (2) the Late Jurassic (J_3) and Early Cretaceous (K_1) deformed volcanic rocks unit (Douling Formation and Nanyuan Formation, respectively), located in the NW side of the CNB, metamorphozed under green schist facies (Chen, 1997; Tong & Tobisch, 1996); (3) the plutons with oriented minerals, including gabbro, diorite, granodiorite, monzogranite and two-mica

granite, intruding into the former two units (Wei et al., 2015). These plutons were also described as weakly deformed plutons (Cui et al., 2013) or syn-tectonic plutons on the basis of their preferred orientation of minerals and microgranular mafic enclaves without sub-solidus deformation, moreover, this orientation is concordant with regional ductile fabrics reported (Li et al., 2003; Tong & Tobisch, 1996; Wei et al., 2015); (4) the undeformed isotropic plutons intruding into the previous rocks. These plutons were featured by a magmatic texture and isotropic structure, among which numerous plutons are of A-type granite with miarolitic texture (Zhao et al., 2016; Zhou et al., 2006); (5) the Late Cretaceous undeformed volcanic rocks unit (Shimaoshan Formation), unconformably overlying the deformed rocks. The undeformed volcanic rocks consist of rhyolite and basalt as bimodal volcanic series, in which there also developed andesite (Qiu et al., 1999; Guo et al., 2012; Li, Li et al., 2018). The volcanic rocks in the CNB, regardless of deformed or not, have magmatic arc affinities (Guo et al., 2012). Besides, the rocks in the CNB were intruded by NE-SW striking mafic dyke swarms coeval with the undeformed volcanic rocks (Dong et al., 2006).

2.3. The geochronological framework of the CNB

Hundreds of zircon U-Pb dating on igneous rocks (volcanic rocks, plutons and orthogneiss) and ^{40}Ar-^{39}Ar dating on whole rock, amphibole, muscovite, biotite and k-feldspar from deformed rocks (deformed volcanic rocks and orthogneiss) have allowed to establish the magmatic activity and cooling age of the CNB (Figures 2a-d; Appendix Table S1). The oldest zircon U-Pb age for the orthogneiss of the CNB was dated at 187 ±1Ma (Liu et al., 2011), while the youngest one yielded U-Pb age of 130±1 Ma (Liu et al., 2012). The oldest pluton with oriented minerals was dated at 132±3 Ma (Zhou et al., 2016), while the youngest one was dated at 105±2 Ma (Xu, 2019). The age of undeformed isotropic granite ranges from 105±1 Ma (Ding et al., 2015) to 82±1 Ma (Huang & Lin, 2019). Contrary to the consistent plutonism without obvious stop, the volcanism is rather episodic (Figures 2b-d). The Nanyuan Formation of the deformed volcanic rocks unit was of 143-130 Ma in age, the undeformed volcanic rocks unit (the Shimaoshan Formation) was of 104-95 Ma in age, therefore there was a volcanic

quiescence between these two volcanic units (Guo et al., 2012). The cooling ages of the deformed rocks by ^{40}Ar-^{39}Ar dating range from 133 Ma to 84 Ma (Wang & Lu, 2000; Chen et al., 2002).

3. Field observation

In the CNB, the plutons with oriented minerals have often a cartographically spindle shape with a NE-SW striking long axis (Figure 2a). Although distributed in a 400 km long belt, these plutons share the similar structural features. In the field, a NE-SW striking highly inclined magmatic foliation has been observed and defined by oriented minerals (Figure 3a), microgranitoid enclaves and schlieren (Figures 3b and c). In the case that the granitoids intruded as dykes, the planar mineral orientation in granitoid dykes, the foliation of the K_1 deformed volcanic rocks, the wavy contacting boundary between the two rocks are parallel with each other (Figure 3d). In the presence of K_1 deformed volcanic rock xenolith, the magmatic foliation surrounds but does not penetrate the xenolith (Figure 3e). In the case that the granitoids intruded as pluton, it could develop a zonal structure characterized by a mylonitic boundary with country rocks (Figure 3f), a rim with magmatic foliation and an isotropic core (Figures 3c and 3g). On the country rock side, the volcanic rocks of the K_1 Nanyuan formation was metamorphozed into hornfels (Figure 3h). The detailed description of field observation on each pluton can be found in supplementary materials (Appendix Table S2).

4. Sampling and analytic method

4.1. Sampling and measurement of AMS

In order to determine the regional tectonic regime during the emplacement of the plutons with oriented minerals in the CNB, AMS sampling has been carried out with gasoline driller. In spite of strong weathering and large urbanization, the sampling was conducted in 39 sites with high outcrop quality from 9 individual plutons covering the whole length of the CNB. For each pluton, efforts were made to ensure the regular distribution of sites with an interval of about 2 km. In each site, 5-6 cores of 2.5 cm in

diameter were acquired and oriented by magnetic compass. When weather permitted, the solar orientation was taken as well to correct geomagnetic declination. In laboratory, the cores were cut into standard cylinder specimen of 2.2 cm in height. Finally, 321 standard cylinder specimens were prepared.

Isothermal Remanent Magnetization (IRM), thermal-susceptibility experiments and AMS were conducted in the Institut des Sciences de la Terre d'Orléans (ISTO; France). The AMS were measured with KLY3 kappabridge. Sample FJ02, FJ24, FJ42, FJ45 and FJ64 were magnetized with IM30 pulse magnetizer at steps of 10 mT, 20 mT, 40 mT, 60 mT, 90 mT, 120 mT, 150 mT, 200 mT, 300 mT, 450 mT, 600 mT, 800 mT and 1000 mT, and measured by JR5 magnetometer after each step of magnetization. The powders of the same samples were heated to 700°C and subsequently cooled to room temperature by CS3 furnace in air, and the susceptibilities were measured with KLY3 kappabridge simultaneously. Hysteresis loops were measured in the Paleomagnetic laboratory of Institut de Physique du Globe de Paris with 1000 mT maximum exerted magnetic field.

4.2. Zircon La-ICP-MS U-Pb dating

In order to acquire the ages of representative plutons with oriented minerals, 4 samples were collected from 4 plutons: FJ08 (Dongzhuang pluton), FJ52 (Suao pluton), FJ53 (Matui stock) and FJ54 (Gaoshan pluton) were dated with zircon by an Aglient 7500a ICP-MS equipped with a 193 nm laser ablation system at the Institute of Geology and Geophysics, Chinese Academy of Sciences (IGGCAS; Beijing). The analytical procedures followed Xie et al. (2008).

Under the microscope, the zircons from four sampled granitoids are transparent, euhedral and prismatic with long axes of crystals ranging between 100 and 150 μm. In the cathodoluminescence (CL) image, the zircons developed oscillatory zoning (Appendix Figure S1a). Twenty-five grains for each sample have been analyzed. "IsoplotR" was used to process U-Pb data (Vermeesch, 2018). During processing, the data with difference between Pb^{207}/U^{235} and Pb^{206}/U^{238} ages larger than 10% are excluded from the calculation of the concordant age. Some data were also rejected by

"IsoplotR" from calculation owing to their large differences with other data.

4.3. Monazite U-Th-Pb microprobe dating

Monazite can crystallize in an Al-rich melt and represent its crystallization age (e.g., Parrish, 1990; Ji et al., 2018). Sample SC236 (two mica granite of the Huian pluton) was chosen for monazite finding and U-Th-Pb microprobe dating in ISTO with Scanning Electricity Microscope (SEM) and Electron Probe Micro Analyzer (EPMA), respectively. The analytical procedure followed Cocherie et al. (1998).

In order to ensure the quality of measurement, all the analyzed monazites were larger than 20 μm. As a result, 17 monazite grains of 30-50 μm in diameter without zonation have been found and measured in SC236 (Appendix Figure S1b). During the measurement, attention was paid to keeping monazite edge away. Individual grain age calculation and data sorting were realized by using an Excel macro of "Macro Monazite" written by Pommier et al. (2003) to get an apparent age of each measurement. With Excel macro of "Isoplot" (Ludwig, 2003), the mean age for the processed sample was reached.

4.4. Zircon Hf isotopic data statistics

From the published articles in English and Chinese literature, zircon Hf isotopic data of the CNB and its adjacent areas (Figure 1) have been collected. Owing to the isobaric interferences of ^{176}Yb on ^{176}Hf, the precise determination of the ^{176}Hf/^{177}Hf ratio was hampered during mass spectrometry analysis (Wu et al., 2006). In order to construct a better magmatic provenance evolution history, zircon Hf isotopic data reported in previous studies were carefully examined and filtered. Those data with linear relationship between ε Hf(t) and ^{176}Yb/^{177}Hf indicate that the Hf isotopic measurement is determined by ^{176}Yb content in the sample, therefore these data were not included in the statistics. Finally, 532 pieces of data in the interior Fujian area and 1787 pieces of data in its coastal Fujian areas were obtained (Appendix Table S3).

5. Result of AMS measurement

5.1 Magnetic carrier

The bulk susceptibilities of the studied granitoids range from 2 to 329×10^{-4} SI (Figure 4a and Appendix Table S4). Thermal-susceptibility curves reveal a rapid decrease at 580°C, and a slow decrease to zero between 600°C to 700°C (Figures 5a-e). Hysteresis loops are sigmoid in shape with weak coercivity, featured by saturation magnetization nearly 1000 mT, and the weakly linear increase of magnetic moment with respect to exerted magnetic field can be neglected (Figures 5f-j). IRM curves rapidly increase to near saturation in the exerted field under 100mT (Figures 5k-o). These phenomena suggest that magnetite is the predominant magnetic carrier, and the contribution of paramagnetic minerals can be neglected. It should be noted that in the thermal-susceptibility experiment, the susceptibility continues to decrease till 680°C after the rapid drop near 580°C. There was a weak coercivity illustrated by hysteresis loop, and a rapid saturation of magnetization in hysteresis loop as well as IRM experiments. All reveal that, in addition to the predominant magnetite, a trivial content of hematite existed in the studied samples.

In the Day-plot diagram, all specimens plot into pseudo-single domain (Figure 4b), suggesting a normal magnetic fabric (Tarling & Hrouda, 1993). Therefore, the magnetic fabrics are comparable with the mineral shape preferred orientation and can be directly used for the petrographic and structural interpretations.

5.2. AMS fabrics

The Corrected Anisotropy Degree (P_J) was used to constrain the anisotropy intensity of AMS (Jelinek, 1981). In the CNB, the site-mean P_J values range from 1.062 (two-mica granite) to 1.624 (granodiorite), and 56% sites have P_J values higher than 1.2 (Appendix Table S4). The P_J value linearly varies with the mean magnetic susceptibility (Km) (Figure 4c). The site-mean shape parameter of AMS ellipsoid (T; Jelinek, 1981) ranges from -0.180 to 0.687, and 90% sites present their T values above zero, indicating that the AMS ellipsoids are predominated by oblate shape.

The AMS data quality can be determined by the radius of the confidence ellipse at

95% probability level as expressed by α_{95max} and α_{95min} (long and short radius of the confidence ellipse for a site-mean statistics of AMS data). For a practical estimation, the mean value of α_{95max} and α_{95min} can be used to distinguish the high quality data (concentrated within a site) with an average α_{95} smaller than 20° from low quality data (scattered within a site; e.g., Charles et al., 2012). Based on this criterion, for the site-mean K_1 data (magnetic lineation), 92% sites were in good quality; while for K_3 data (pole of magnetic foliation), 97% sites were in good quality (Appendix Table S4 and Figure 6). Therefore, the structural analysis can be confidently conducted with these AMS data. Generally speaking, in the whole CNB, regardless of the location, lithology, emplacement time or size of the plutons, the magnetic lineations of studied granitoids are clustered within one site, and scattered at the pluton scale; while their magnetic foliations are clustered, highly inclined, and NE-SW striking both in site and pluton scales (Figure 6). The distribution pattern of magnetic foliation is consistent with the observable magmatic foliation of the pluton and the ductile foliation of the country rocks nearby (Figures 2, 3 and 6). For example, in the Su'ao (Fj52, Figure 6), Matui (Fj53, Figure 6), Gaoshan (Fj54, Figure 6), Dongzhuang (Fj05-Fj08, Figure 6), Huian (FJ21, FJ65-67, Figure 6) plutons and the Longshoushan stock (Fj84, Figure 6), the magnetic foliation is parallel to the orientation of the rock-forming minerals, microgranitic enclaves and schlieren (Figures 3a-c and 6). On the southern boundary of the Hui'an granite, the magnetic foliation is parallel to the orientation of rock-forming minerals, microgranitic enclaves, schlieren (Figure 3c) and ductile foliation (Figure 3f). In its center, although no magmatic fabrics are observable by eyes in the field, the magnetic foliations are still clustered in the NE strike with steep inclinations (e.g., FJ43, FJ57 and FJ62 in Figure 6).

6. Microscopic observations

In order to determine the acquisition mechanism of the AMS and observe the microscopic response to the regional tectonic events during the emplacement of the studied plutons, oriented thin-sections have been made along the direction parallel to

the magnetic lineation and perpendicular to the magnetic foliation (XZ section) from the AMS standard cylinder specimens. Moreover, for those specimens in which the NE-SW shallow inclined magnetic lineation developed, the oriented thin-sections perpendicular to the magnetic lineation and perpendicular to the magnetic foliation (YZ section) were also made. Finally, two kinds of thin section were acquired, namely, a NW-SE-striking vertical plane and a horizontal plane.

Microscopic features of the studied plutons are highly consistent. All of them present rock-forming minerals with their long axes parallel to the strike of magnetic foliation (Figure 7). Along the feldspar boundary, myrmekite is frequently developed (Figures 7a and g). The feldspar grains present sutured boundaries with each other or with quartz grains (Figures 7b, c, d, f, h), indicating a grain boundary migration recovery (Passchier & Throw, 2005). The completed and uncompleted transected cracks developed in feldspars were filled with quartz and muscovite, representing the residual melt (Figures 7d and e). Quartz grains developed wavy extinction, subgrains, chessboard structure, rectangular shape or suture-shaped boundary with each other (Figure 7). The biotite was bent (Figure 7d), and, sometimes developed as feldspar pressure shadows around feldspar containing tiny quartz grain inclusions (Figure 7b).

7. Geochronology results

For zircon U-Pb La-ICPMS dating, as a result, 25, 16, 13 and 20 measurements were adopted to calculate ages for FJ08, FJ52, FJ53, FJ54, respectively (Figures 8a-d). All the measurements were featured by Th/U ratio larger than 0.1 that agrees with the magmatic crystallization origin of zircon grains (Appendix Table S5; Rubatto, 2002). The magma crystallization ages were determined at 118Ma, 122Ma, 127Ma and 118Ma for samples FJ08 (granodiorite of the Dongzhuang composite pluton), FJ52 (biotite monzogranite of the Su'ao pluton), FJ53 (biotite monzogranite of the Matui stock) and FJ54 (biotite monzogranite of the Gaoshan pluton), respectively (Figures 8a-d) with MSWD values less than 1.8 and errors less than 1.57 Ma.

Finally, 265 monazite apparent ages were calculated based on the measurement

results (Fig. 8e). The average age of the magma crystallized monazite from sample SC236 (two mica granite of the Huian composite pluton) was calculated at 119.6±2.1 Ma with a MSWD value of 1.07 (Figure 8e; Appendix Table S6).

8. Discussion

8.1. Origin and bearing of fabrics of the studied plutons

Primary fabrics of igneous rocks are those associated with the emplacement before the final crystallization of a pluton and secondary fabrics refer to those acquired posterior to the final crystallization. However, to distinguish these two kinds of fabrics is sometimes difficult, especially in the condition of emplacement under a stressed environment (Tarling & Hrouda, 1993). Nevertheless, the AMS data with low P_J values are often considered to be acquired during the magmatic intrusion rather than posterior deformation (Tarling & Hrouda, 1993). Studies also indicated that P_J value can be used as strain intensity gauge in the finite-strain zone and ferromagnetic granites since it is increased with deformation/strain degree in a precondition of no relationship between P_J value and Km (Tarling & Hrouda, 1993; Sen et al., 2005; Tripathy, 2009). Although the P_J value of the studied granites is high (e.g., Lyra et al., 2018), considering that it varies with Km in this study (Figure 4c), the high P_J value indicates higher concentration of magnetite in measured samples rather than evidence of posterior deformation superimposition (e.g., Rochette et al., 1992; Wei et al., 2014). According to the discrimination criteria established by previous studies (e.g., Bouchez & Gleizes, 1995; Paterson et al., 1998; Vernon, 2000), the fabrics of the studied plutons in the CNB can be considered as primary ones acquired before their melt final crystallization, with the following field evidences: (1) widely distributed mineral orientations and schlieren without plastic deformation (Figures 3a-c); (2) magmatic flow foliations deflected around xenoliths indicating that magma flowed around solid objects (Figure 3e); (3) widely distributed oriented microgranitoid enclaves without plastic deformation of crystals indicating that they flowed as magma globules (Figures 3b and c).

Microscopically, numerous observations indicate that the fabrics of the studied

granites developed in supra/near-solidus conditions with the presence of residual melt, meaning that the fabrics are primary: (1) a high temperature recovery (Grain Boundary Migration) near solidus condition including suture shaped boundaries between quartz and feldspar grains (Figure 7; Passchier & Throw, 2005); (2) a chessboard structure and rectangular shape of quartz indicating a high temperature plastic deformation (Figures 7c and h; Passchier & Throw, 2005); (3) well-oriented feldspars with widely developed wedge-shaped and uncompleted transected cracks infilled with late stage crystallized minerals, such as quartz and muscovite (Figures 7d and e; Bouchez et al., 1992); (4) late stage magmatic minerals such as quartz developed in biotite as "pressure shadows" on the end of plagioclase. In this structure, biotite “pressure shadow” and plagioclase define the fabric (Figure 7b; Vernon et al., 2000 and enclosed references).

The primary fabrics can be originated from thermal convection of magma or regional tectonic impact (Tarling & Hrouda, 1993). The magma can develop a convection fabric by intrusion without disturbing from the regional stress (tectonic quiescence setting; e.g., De Oliveira et al., 2010); or in a fast intrusion and cooling in which the regional stress has not enough time to accumulate its effect on strain (intrusion of dyke, pluton construction by means of coalescence of acidic dykes or pluton emplacement in shallow depth; e.g., Raposo & Ernesto, 1995; Turrillot et al., 2011; Wei et al., 2014). However, several facts indicate that the influence from the regional stress on the studied plutons during their emplacement cannot be ruled out: the contemporaneous regional deformation in the CNB, the important intrusion depth of the studied plutons and no evident structure showing a coalescence of dykes (Tong & Tobisch, 1996; Wei et al., 2015). Furthermore, the following observations argue for the view that the fabrics are results of regional stress, in other words, the studied granitoids are syn-tectonic plutons: (1) the good consistency between the magmatic foliations of granitic dykes, the ductile foliation of the deformed volcanic rocks, and the smooth and concordant wavy boundary between these two rocks indicate that the viscosity contrast between these two rocks was weak, and granitic dyke intruded coevally with the deformation of volcanic rocks (Figure 3a; Paterson et al., 1998; Pitcher, 1979); (2) the high consistency between the magmatic/magnetic fabrics from numerous plutons along

the 400-km-long Channgle-Nan'ao belt and the regional ductile foliation recorded in the country rocks indicates that the former is most likely caused by a regional tectonic event (Figures 2 and 6; Paterson et al., 1998); (3) typical structures of syn-tectonic plutons are observed in the studied plutons (e.g., Zak et al., 2005). For instance, the Hui'an pluton (Location 7 in Figure 2) with an isotropic core (Figure 3g), an undeformed rim with oriented minerals (Figure 3c), and a mylonitic boundary with host rocks (Figure 3f). The rim of oriented minerals and the isotropic core in the Damaoshan (Location 10 in Figure 2) and Duxun (Location 13 in Figure 2) plutons imply that the melt crystallization was influenced by the regional-scaled tectonics; (4) The high temperature ductile deformation/recovery and cracks with presence of residual melt, as discussed above, suggest a crystallization under near solidus stress (Bouchez et al., 1992; Hibbard, 1987; Passchier & Throw, 2005; Paterson et al., 1998).

In summary, the fabrics developed in the studied plutons were acquired in the sub-magmatic condition near solidus under a regional tectonic control. Therefore, they can be considered as syn-tectonic granitoids and will shed light on the regional tectonic regime during their emplacement.

8.2. Strain and stress field implications for the CNB The tectonic regime of the CNB has long been debated, although it is crucial to understand the geodynamic background of the EACM during the Late Mesozoic. The CNB was considered as a continental-scaled sinistral strike-slip fault produced by the northward drifting of the Paleo-Pacific plate (Charvet et al., 1990; Xu et al., 1987). Structural analyses indicated that there was a kinematic change from sinistral to dextral due to the drift direction change of the Min-Tai microcontinent (the Gneiss Unit in this study) that collided with the Min-Zhe volcanic arc (the Deformed Volcanic Rocks Unit in this study) during the Early Cretaceous (Wang & Lu, 1997). Paleomagnetic results from dykes in Hong Kong indicated that there was a clockwise rotation of the SE coast area of the SCB with respect to the SCB, therefore this argued for a dextral strike-slip movement along the CNB (Li et al., 2005). In recent years, structural analyses on ductile deformation with large covering on the CNB emphasized that the Gneiss Unit thrusted to the NW above

the Deformed Volcanic Rocks Unit (Wei et al., 2015).

In this study, a regional tectonic evolution is reconstructed by an integrated AMS and macro-micro deformation analysis on the syn-tectonic plutons.

In the entire CNB, the magmatic/magnetic foliations of the syn-tectonic granitoids are highly clustered with the NE striking and steep inclination (Figures 2 and 6), suggesting a NW-SE shortening (e.g., Roman-Berdiel et al., 1998; Zak et al., 2009), in agreement with the predominant oblate AMS ellipsoid shape illustrated by positive T values.

Owing to the fact that the magmatic/magnetic fabrics of syn-tectonic pluton were formed in the near-solidus status, the crystal content in magma is high enough to directly contact each other and, therefore, can transmit stress (Paterson et al., 1998 and enclosed references). In this case, a stressed crystal in a magma mush will tend to rotate to have its flattest face perpendicular to the maximum shortening direction (Z axis) interpreted as the maximum principal stress vector (σ_1; e.g., DeVore, 1969; Paterson et al., 1998). Therefore, the dominant NE-striking and deeply inclined magmatic/primary magnetic foliation suggest a NW-SE shortening. The myrmekite structure developed along the NE-SW striking and the vertically arranged feldspars also support a NW-SE shortening direction (Figures 7a and g; Simpson & Wintsch, 1989). This analysis of the strain and stress fields is further supported by the horizontal cracks developed perpendicularly to the maximum stretching direction (X axis), interpreted as the minimum principal stress axis (σ_3; Figure 7a, e-f; Bouchez et al., 1992).

The NW-SE shortening regime deduced from these field observations and petro/magnetic fabrics is consistent with the NW-directed thrusting event revealed by the regional-scaled ductile deformation (Wei et al., 2015).

8.3. Timing of the NW-SE shortening event in the CNB

The deformation time of the CNB has long been debated. In order to constrain the deformation age of the CNB, numerous Ar^{40}-Ar^{39} dating on whole rock, amphibole, biotite, muscovite and K-feldspar have been carried out with a range from 132 to 84 Ma (e.g., Wang & Lu, 2000; Chen et al., 2002). However, some scholars argued that

Ar^{40}-Ar^{39} ages could have been reset by the extensive posterior magmatism and, therefore, suggested that the emplacement age of syn-tectonic granites would be more suitable for representing the deformation age of the CNB (Li et al., 2003). The statistics of zircon U-Pb ages of plutons and Ar^{40}-Ar^{39} ages reveal that the peak of Ar^{40}-Ar^{39} ages is coincident with the peak of the magmatic ages at around 100 Ma confirming the reset of Ar^{40}-Ar^{39} timer (Li et al., 2015). Moreover, the similarity between the Ar^{40}-Ar^{39} ages of gneiss and those of the nearby plutons favors this argument (e.g., Location 12 in Figure 2).

In this study, zircon and monazite dating have been conducted on the syn-tectonic granitoids documented by our structural analyses. The correlation of dating between the previous study and this study suggests that the time interval between the oldest and youngest ages of the syn-tectonic plutons ranges from 131Ma to 105 Ma (Figure 2; Li et al., 2003; Xu, 2019). Taking the dating error into consideration, this time window is comparable to the age of the youngest deformed volcanic rocks and the age of the oldest undeformed volcanic ones at 130 Ma and 104 Ma respectively (Guo et al., 2012). Therefore, the Cretaceous NW-SE compressional regime in the CNB lasted from 130 to 105 Ma.

8.4. Geodynamic implications

8.4.1 Collision between the SCB and DGWP

The magmatism and deformation in the CNB were once considered to be response to the Paleo-Pacific slab subduction (Chen et al., 2002; Xu et al., 1987). Furthermore, the chaotic clastic sequence with Middle, Late Jurassic and Early Cretaceous exotic blocks recognized in the Calamian and NE Palawan islands of West Philippines area was interpreted as the accretionary prism of the Cretaceous Paleo-Pacific slab subduction (Figure 1b; Faure & Ishida, 1990; Zamoras & Matsuoka, 2004). However, several lines of evidence indicate that this chaotic clastic sequence with exotic blocks was formed in a collision-involved setting: (1) in the Mindoro Island located in the northern part of DGWP, K_1 ophiolites were developed and overlain by the chaotic sequence (Faure et al., 1989; Yumul et al., 2007). To the north, geometrically above this

ophiolite, crops out a Permian pluton that can be correlated with the Permian ones in the SCB (Knittel et al., 2010). While to its south, geometrically below this ophiolite, gneisses representing the continental basement of the DGWP are exposed (Faure et al., 1989). It should be noted that there also developed Cenozoic ophiolite in this island (Figure 2d; Yumul et al., 2007). The eastern part of the Mindoro Island belongs to the East Philippine Mobile Zone in which accretionary complex with several ophiolitic belts developed (Yumul et al., 2007). These ophiolitic belts are featured by a west-younging age trend with the Jurassic one in the east and the Cenozoic one in the west (Yumul et al., 2007). This trend suggests that in the Mindoro Island, the ophiolitic belt with the Cenozoic age is the suture zone between the DGWP and East Philippine Mobile Zone, while it is better to interpret the K_1 ophiolitic zone as a nappe rooted in the suture zone located between the SCB and DGWP; (2) Considering the clockwise rotation of the DGWP due to the opening of the South China Sea (Figure 1), the 130-105Ma NW-directed thrusting in the CNB in the SCB (Wei et al., 2015) can be correlated with the S-directed thrusting in West Philippines (Faure et al., 1989) and the 123-104 Ma S-directed thrusting deformation documented by the geometry/kinematic data from seismic imaging and geochronology/petrology data from dragged ductily sheared samples of amphibolite, paragneiss, garnet-mica schist in the Reed Bank (Kudrass et al., 1986; Liang et al., 2019); (3) Seismic imaging of high resolution across the southern flank of the South China Sea spreading center reveals a northward increase of shortening ratio of the Mesozoic strata from the NW Borneo trough (Nansha trough) to the area near the spreading center zone, from about 3% to 9% respectively (Figure 1a; Zhu et al., 2018). This indicates that the major deformation is located along the nowadays South China Sea spreading center and the Mindoro K_1 ophiolitic zone between the SCB and DGWP, compatible with the collision that occurred here (Faure et al., 1989; Hall, 2009, 2012), rather than the accretionary process that occurred on southern flank of the DGWP (Zamoras & Matsuoka, 2004).

8.4.2 Collision time

The collision time between the SCB and DGWP is inconclusive yet. Due to that the arc-related magmatism was ended ~80 Ma, it was proposed that the collision

between the SCB and DGWP occurred during the K_2 along the suture line located in the nowadays South China Sea spreading center (Hall, 2009, 2012). This hypothesis was questioned since the Late Cretaceous deformation and metamorphism have not been observed in this zone (Morley, 2012). Based on our observations, a K_1 collision occurring during 130-105 Ma is suggested by the following arguments: (1) the K_1 age of ophiolite marks the lower time limit of the collision. The chaotic clastic sequence with exotic blocks ended at the K_2 and then terrigenous formations were developed with clast supply from the SCB, showing that the SCB and DGWP blocks were already close to each other at that time (Suggate, 2014). Their close paleogeographic positions during the Cretaceous were also revealed by paleomagnetic records (Almasco et al., 2000); (2) the 130-105 Ma NW-SE shortening regime in the CNB evidenced by the development of NW-thrust (Wei et al., 2015) and emplacement of syn-tectonic granitoids revealed in this study account for the K_1 time of the collision; (3) widely distributed K_1/K_2 unconformity in the eastern SCB, northern and southern banks of the South China Sea also support a K_1 time for the collision (Shu et al., 2009; Yan & Liu, 2004; Yao et al., 2011; Zhang et al., 2015).

8.4.3 Syn-collisional plutonism in the CNB

It should be noted that the SCB was generally characterized by a 130-105 Ma magmatic lull during the K_1 collision period (Figure 1c). On the contrary to this general feature of magmatic quiescence, there still developed plutonism in the CNB (Figures 2b and 9a). During this time span, the CNB was largely affected by mantle activities evidenced by mafic gabbro pluton emplacements (Figures 2a and d), injections of mafic magma into acidic-intermediate granitoids (micro-granitoids enclave, schlieren; Figure 3) and positive zircon ε Hf(t) of granitoids (Figure 9a; e.g., Kemp et al., 2009). The compiled Late Mesozoic zircon ε Hf(t) data from the CNB and its adjacent areas indicated a 3-stage Hf isotropic evolution for the coastal Fujian area (Figure 9a; Appendix Table S3), namely, Stage 1 (pre-collision to 125 Ma): the ε Hf(t) values were predominantly negative; Stage 2 (125-105 Ma): the ε Hf(t) values abruptly

increased and became highly positive; Stage 3 (105-80 Ma): the ε Hf(t) values showed a decrease trend. In contrast, the plutonic rocks in the interior Fujian area always showed negative ε Hf(t) values, and during 125-110 Ma, there was a magmatic gap, probably corresponding to the collision (Fig. 9b).

In an active continental margin, after the complete subduction of an oceanic slab, the arrival of a (micro)continent in the subduction zone will lead to slab break-off due to the tensional stress caused by the dense subducted oceanic slab and the buoyancy of less dense continental block (Magni et al., 2013). Numerical modeling indicated that the slab necking and break-off began to occur usually 2-20 Ma after the initial collision (van Hunen & Miller, 2011 and references enclosed). Owing to the foundering of the detached slab, the mantle convection was disturbed, leading to mantle upwelling, heating of continental lithosphere, and magmatic activity with mantle material signature (e.g., Ji et al., 2016).

In the Late Mesozoic period, from ~130 to 105 Ma, the mantle derived magma intrusion documented by gabbro, mafic enclave and schlieren in the studied plutons was coincident with the collision (Figures 2a and d). Moreover, the 5 Ma delay of abrupt increase of ε Hf(t) values with respect to the initial collision suggests a possible causal relationship between the mantle upwelling and collision. Furthermore, this syn-collision magmatism is restricted around the narrow CNB belt whereas in the interior Fujian area the contemporaneous magmatism was absent (Figures 1a, 9b), suggesting a linear distribution of magmatism after the initial collision. The slab break-off subsequent to the collision may be a reasonable controlling factor. It is interesting to note that coeval with the syn-collision plutonism, the volcanic activity ceased (Figures 2b and 2c). Probably it was due to the fact that a volcanic eruption requires the opening of magma conduits connecting magma chamber to the surface. Such a conduit is easily opened in an extensional regime (Nédélec et al., 2015). It is therefore suggested that the 130-105 Ma NW-SE collision-related shortening regime is responsible for the absence of magmatic conduits and related volcanic eruption. Previous geochemical studies argued for the 120-110 Ma mafic magmatism with an arc affinity in an advancing subduction setting (Guo et al., 2021). Their arguments seemed to be in

agreement with the high water content for this amphibole-bearing gabbro (e.g., Griffin et al., 2002; Li, Wang et al., 2018). However, the continuous single subduction all through the Late Mesozoic without collision and subsequent slab break-off cannot explain the magmatic provenance change before and after 125 Ma revealed by gabbro intrusion, abrupt ε Hf(t) value increase in the coastal Fujian area (Figures 2d and 9a) and the lines of evidence for the above discussed collisional model. Considering that the collision of two continental blocks will significantly decrease the inter-plate convergent velocity, a newly formed subduction could be triggered on the rear of the arriving subducted continent block (Figure 10; e.g., Li and Li, 2007). During the 130-105 Ma collision, the water-rich environment could be maintained by the newly formed NW-directed Paleo-Pacific slab subduction on the southeastern flank of the DGWP (subduction jump).

8.4.4 Cretaceous tectonic evolution model of the SCB

Integrating the structural analyses, geochronologic results, petro/AMS patterns and geochemical data, a 3-stage tectonic evolution model can be proposed to reconstruct the history of the Paleo-Pacific slab subduction and the tectonic consequence in the CNB, SCB and their adjacent areas during the Cretaceous.

Stage 1. From the beginning of the Cretaceous to 130Ma (Figure 10a), the Paleo-Pacific slab subducted beneath the EACM leading to the back-arc magmatism represented by igneous rocks of the Deformed Volcanic Rocks Unit and the Gneiss Unit in the CNB. The negative ε Hf(t) values suggest that continental sediments were subducted from the oceanic trench to the mantle (Kemp et al., 2009; Figures 9a and 10a). Although no extensional structures were reported in the CNB by previous studies, possibly due to the important tectonic reworking of Stage 2, the bimodal volcanic series (Li et al., 2009), the widely distributed Early Cretaceous graben and half graben basins (e.g., Shu et al., 2009; Wei et al., 2016 and 2018), and normal faults (Wei et al., 2016 and 2018; Chu et al., 2019) in the SCB argue for an extensional regime.

Stage 2. From 130 to 105Ma (Figure 10b), the DGWP collided with the SCB along the suture zone outcropped in North Mindoro (Figure 1a). Consequently, in the CNB as

the upper plate, there developed a back-thrust-fault system (Wei et al., 2015). The plutons and volcanic rocks previously developed in Stage 1 were pervasively deformed and metamorphized to form the Gneiss Unit and Deformed Volcanic Rocks Unit, and the NE-striking foliation and NW-SE lineation with top-to-the NW shear sense developed during this time. Five Ma after the initial collision, the subducted (Paleo-Pacific) plate experienced a break-off leading to the opening of slab window (e.g., Magni et al., 2013). The asthenosphere up-welling through the slab window allowed mantle melting, and the supply of juvenile materials adds into the upper continental (SCB) crust, as suggested by the rapidly increased positive ε Hf(t) values (Figures 9a and 10b). Moreover, the mantle heat convection raised the temperature of the CNB crust, and caused its partial melting. The newly generated melts were emplaced at depth to form syn-tectonic granitoids in the CNB. On the SE flank of the DGWP, a newly formed Paleo-Pacific slab subduction may provide water to the mantle beneath the CNB, which may also reinforce the syn-collision magmatism. This subduction may have continued till the arrival of the mid-ocean ridge between the Paleo-Pacific slab and the Pacific slab at ~50 Ma (Kimura et al., 2019) and play an important role in the succeeding stage of the tectonic evolution of the CNB and SCB.

Stage 3. During the period of 105-80 Ma, the regional tectonic regime became a NW-SE extension evidenced by the NE-SW striking mafic dyke swarms (Dong et al., 2006), the K_2 half graben basins in the East and South China Sea and SCB with related NE-SW striking boundary normal faults (Shu et al., 2009; Cukur et al., 2011), the bimodal volcanic eruption and A-type granite emplacement in the CNB (Qiu et al., 1999; Zhou et al., 2006; Zhao et al., 2015 and 2016; Li, Li et al., 2018). Given the arc-affinity of mafic rocks during this time, this extension may have been produced by the roll-back and retreat of the newly formed Paleo-Pacific slab subduction on the SE flank of the DGWP. The arrival of this new subduction might shelter the slab window, and consequently, the asthenosphere upwelling was weakened as indicated by the decreasing trend in ε Hf(t) values (Figures 9a and 10c).

8.5. Implications for magmatic tempo The cause of the magmatic tempo has long been

discussed, emphasizing either the tectonic control of overriding plate (Armstrong, 1988; Ducea et al., 2015) or the subduction of underlying plate (Huang & Lundstrom, 2007; Zhang et al., 2019). The former thought is based on the coincidence of magmatic flare-up and shortening regime with thickened crust as shown in the Gangdese batholith, Sierra Nevada batholith and Andes cordillera (Ducea et al., 2015; Paterson & Ducea, 2015). The latter proposed that the high subduction velocity and the subduction roll-back and retreat caused the magmatic flare-up (Huang & Lundstrom, 2007; Zhang et al., 2019). The Cretaceous tectonic evolution of the East Asia Continental Margin provides a test of these claims.

As discussed above, during the Cretaceous, the SE-ward roll back and retreat of the Paleo-Pacific slab subduction caused a general extension and coeval magmatism along the EACM (Sagong et al., 2005; Li & Li, 2007; Wu et al., 2007 and 2019). Probably due to the collision of the DGWP with the SCB, this extension was interrupted in the SCB. Moreover, due to the limited size of the DGWP, when the collision occurred only in the active continental margin of the SCB, the northern segment of the EACM was still featured by extension and 130-120 Ma magmatic flare-up in North China, Korean Peninsula and Japanese Islands (Fig. 1b; Sagong et al., 2005; Li & Li, 2007; Wu et al., 2007 and 2019). The 3-stage tectonic evolution of the SCB, including the 145-130 Ma extension, the 130-105 Ma shortening and the 105-80 Ma extension, corresponds respectively to the flare-up, the lull and the flare-up magmatic activities in this area (Figure 2c). During the collision, the fold and thrust belt developed (Wei et al., 2015) and the crust was thickened to ~42 km (Guan & Wang, 2017). Therefore, this study seems to have provided a counter case for the claims of shortening regime as the first order cause for magmatic flare-up. Instead, in the case of the EACM, the roll back and retreat of underlying subduction slab probably is the major cause for the flare-up during the Cretaceous while the shortening event leads to the magmatic lull.

9. Conclusions

Analyses of data from the present multidisciplinary study, encompassing field observation, AMS measurement, microscopic textural observation, geochronological

study, regional geologic correlation, and zircon ε Hf(t) evolution, have provided answers concerning the magma genesis, tectonic and geodynamic settings of emplacement of syn-tectonic plutons in the CNB. We therefore can reach the following conclusions.

1, The plutons with oriented minerals are syn-tectonic and emplaced under a NW-SE shortening tectonic regime due to the collision between the SCB and DGWP; 2, This collision was geochronologically constrained between 130 and 105 Ma as documented by the emplacement timing of these syn-tectonic plutons;

3, Accommodating with this collision, a slab-break off and a slab window opening might occur, and an asthenospheric upwelling was probably generated below the CNB. This supplied heat in the upper plate, causing partial melting and granitoids emplacement under a shortening regime in the CNB. This may explain why the contemporary magmatism was less developed quasi in the whole SCB due to the limited distribution of the slab window;

4, The tectonic evolution and coeval magmatic activities of the SCB indicated that the shortening regime and thickened crust of the overriding plate may not be the major cause of the magmatic flare-up. Instead, this study has lent support to the view that the roll back and retreat of the underlying subduction slab may cause the magmatic flare-up of the EACM during the Cretaceous.

Acknowledgement

We are grateful to Drs. Song Yifan, Wang Hao, Zhang Xiaoran, Chen Jingyuan and Professors Guo Jinghui, Guo Shun and Ji Weiqiang, who have offered opinions for interpreting Hf isotope and break-off data during a discussion of this study. We benefit a lot from suggestions and refinements of the Associate Editor Daniel Pastor-Galán and the two anonymous reviewers. This study was jointly funded by projects of the National Natural Science Foundation of China (91855212, 41502215), and the Open foundation of Shanghai Sheshan National Geophysical Observatory (2020K08).

Data Availability Statement

The supporting information of Table S1-S6, Figure S1 and Excel Macro "Isoplot" using for monazite age calculating can be found in the webpage of https://doi.org/10.6084/m9.figshare.21455865. The tool of "IsoplotR" with which the zircon U-Pb data was processed can be found in the webpage of http://www.isoplotr.com/isoplotr/.

References

Almasco, J., Rodolfo, K., Fuller, M., and Frost, G. (2000). Paleomagnetism of Palawan, Philippines, *Journal of Asian Earth Sciences*, *18*(3), 369-389.

Armstrong, R. L. (1988). Mesozoic and early Cenozoic magmatic evolution of the Canadian Cordillera, *Special Paper of the Geological Society of America*, *218*, 55-92.

Bouchez, J. L., Delas, C., Gleizes, G., Nedelec, A., and Cuney, M. (1992). Submagmatic microfractures in granites, *Geology*, *20*(1), 35-38, doi:10.1130/0091-7613(1992)020<0035:smig>2.3.co;2.

Bouchez, J. L., and Gleizes, G. (1995). 2-stage deformation of the Mont-Louis-Andorra granite pluton (Variscan Pyrenees) inferred from magnetic-susceptibility anisotropy, *Journal of the Geological Society*, *152*, 669-679.

Charles, N., Gumiaux, C., Augier, R., Chen, Y., Faure, M., Lin, W., and Zhu, R. (2012). Metamorphic Core Complex dynamics and structural development: Field evidences from the Liaodong Peninsula (China, East Asia), *Tectonophysics*, *560 – 561*, 22-50, doi:http://dx.doi.org/10.1016/j.tecto.2012.06.019.

Charvet, J., Faure, M., Xu, J. W., Zhu, G., Tong, W. X., and Lin, S. F. (1990). The Changle-Nanao tectonic zone, south east china, *Comptes Rendus De L'Academie Des Sciences Serie II*, *310*(9), 1271-1278.

Charvet, J., Shu, L. S., Shi, Y. S., Guo, L. Z., and Faure, M. (1996). The building of south China: Collision of Yangzi and Cathaysia blocks, problems and tentative answers, *Journal of Southeast Asian Earth Sciences*, *13*(3-5), 223-235, doi:10.1016/0743-9547(96)00029-3.

Chen, B. (1997). Petrographic Evidences and Tectonic Significance for Two Phases of Metamorphism in Sillimanite- and Garnet- Bearing Mica Schists of Pintan-Dongshan Metamorphic Zone of Eastern Fuj ian, China, *Acta Petrologica Sinica*, *13*(3).

Chen, W. S., Yang, H. C., Wang, X., and Huang, H. (2002). Tectonic setting and exhumation history of the Pingtan-Dongshan Metamorphic Belt along the coastal area, Fujian Province, Southeast China, *Journal of Asian Earth Sciences*, *20*(7), 829-840, doi:Pii s1367-9120(01)00066-910.1016/s1367-9120(01)00066-9.

Chu, Y., Lin, W., Faure, M., Xue, Z. H., Ji, W. B., and Feng, Z. T. (2019). Cretaceous Episodic Extension in the South China Block, East Asia: Evidence From the Yuechengling Massif of Central South China, *Tectonics*, *38*(10), 3675-3702, doi:10.1029/2019tc005516.

Cocherie, A., Legendre, O., Peucat, J., and Kouamelan, A. (1998). Geochronology of polygenetic monazites constrained by in situ electron microprobe Th-U-total lead determination: implications for lead behaviour in monazite, *Geochimica et Cosmochimica Acta*, *62*(14), 2475-2497.

Cui, J. J., Zhang, Y. Q., Dong, S. W., Jahn, B. M., Xu, X. B., and Ma, L. C. (2013). Zircon U-Pb geochronology of the Mesozoic metamorphic rocks and granitoids in the coastal tectonic zone of SE China:

Constraints on the timing of Late Mesozoic orogeny, *Journal of Asian Earth Sciences*, *62*, 237-252, doi:10.1016/j.jseaes.2012.09.014.

Cukur, D., Horozal, S., Kim, D. C., and Han, H. C. (2011). Seismic stratigraphy and structural analysis of the northern East China Sea Shelf Basin interpreted from multi-channel seismic reflection data and cross-section restoration, *Marine and Petroleum Geology*, *28*(5), 1003-1022, doi:10.1016/j.marpetgeo.2011.01.002.

De Oliveira, D. C., Neves, S. P., Trindade, R. I. F., Dall'Agnol, R., Mariano, G., and Correia, P. B. (2010). Magnetic anisotropy of the Redencao granite, eastern Amazonian craton (Brazil): Implications for the emplacement of A-type plutons, *Tectonophysics*, *493*(1-2), 27-41, doi:10.1016/j.tecto.2010.07.018.

DeVore, G. W. (1969). Preferred mineral distributions of polymineralic rocks related to nonhydrostatic stresses as expressions of mechanical equilibrium, *Journal of Geology*, *77*, 26 – 38.

Ding, C., Zhao, Z., Yang, J., Zhou, H., Sheng, D., Hou, Q., and Hu, Z. (2015). Geochronology, geochemistry of the Cretaceous granitoids and mafic to intermediate dykes in Shishi area, coastal Fujian Province, *Acta Petrologica Sinica*, *31*(5), 1433-1447.

Dong, C. W., Zhang, D. R., Xu, X. S., Yan, Q., and Zhu, G. Q. (2006). SHRIMP U-Pb Dating and lithogeochemistry of basic-intermediate dike swarms from Jinjiang, Fujian Province, *Acta Petrologica Sinica*, *22*(6), 1696-1702.

Ducea, M. N., and Barton, M. D. (2007). Igniting flare-up events in Cordilleran arcs, *Geology*, *35*(11), 1047-1050, doi:10.1130/g23898a.1.

Ducea, M. N., Paterson, S. R., and DeCelles, P. G. (2015). High-Volume Magmatic Events in Subduction Systems, *Elements*, *11*(2), 99-104, doi:10.2113/gselements.11.2.99.

Faure, M., and Ishida, K. (1990). The Mid-Upper Jurassic olistostrome of the west Philippines: a distinctive key-marker for the North Palawan block, *Journal of Asian Earth ences*, *4*(1), 61-67.

Faure, M., Lepvrier, C., Nguyen, V. V., Vu, T. V., Lin, W., and Chen, Z. (2014). The South China block-Indochina collision: Where, when, and how?, *Journal of Asian Earth Sciences*, *79*(2), 260-274.

Faure, M., Marchadier, Y., and Rangin, C. (1989). Pre-eocene synmetamorphic structure in the mindoro-romblon-palawan area, west philippines, and mplications for the history of southeast asia., *Tectonics*, *8*(5), 963-979.

Fyhn, M. B. W., Pedersen, S. A. S., Boldreel, L. O., Nielsen, L. H., Green, P. F., Dien, P. T., Huyen, L. T., and Frei, D. (2010). Palaeocene-early Eocene inversion of the Phuquoc-Kampot Som Basin: SE Asian deformation associated with the suturing of Luconia, *Journal of the Geological Society*, *167*(2), 281-295, doi:10.1144/0016-76492009-039.

Griffin, W. L., Wang, X., Jackson, S. E., Pearson, N. J., O'Reilly, S. Y., Xu, X. S., and Zhou, X. M. (2002). Zircon chemistry and magma mixing, SE China: In-situ analysis of Hf isotopes, Tonglu and Pingtan igneous complexes, *Lithos*, *61*(3-4), 237-269, doi:Pii s0024-4937(02)00082-810.1016/s0024-4937(02)00082-8.

Guan, W., and Wang, Y. (2017). Petrogeochemical Methods for Quantitative Estimation of the Crustal Thickness of Orogenic Belt: Overview and Case Studies, *Journal of Earth Sciences and Environment*, *39*(2), 214-224.

Guo, F., Fan, W. M., Li, C. W., Zhao, L., Li, H. X., and Yang, J. H. (2012). Multi-stage crust-mantle interaction in SE China: Temporal, thermal and compositional constraints from the Mesozoic felsic volcanic rocks in eastern Guangdong-Fujian provinces, *Lithos*, *150*, 62-84, doi:10.1016/j.lithos.2011.12.009.

Guo, F., Wu, Y., Zhang, B., Zhang, X., Zhao, L., and Liao, J. (2021). Magmatic responses to Cretaceous subduction and tearing of the paleo-Pacific Plate in SE China: An overview, *Earth-Science Reviews*, *212*, doi:10344810.1016/j.earscirev.2020.103448.

Hall, R. (2009). Sundaland: Basement character, structure and plate tectonic development, paper presented at Thirty-Third Annual Convention.

Hall, R. (2012). Late Jurassic-Cenozoic reconstructions of the Indonesian region and the Indian Ocean, *Tectonophysics*, *570*, 1-41, doi:10.1016/j.tecto.2012.04.021.

Hall, R. (2013). Contraction and extension in northern Borneo driven by subduction rollback, *Journal of Asian Earth Sciences*, *76*, 399-411, doi:10.1016/j.jseaes.2013.04.010.

Hennig-Breitfeld, J., Breitfeld, H. T., Sang, D. Q., Vinh, M. K., van Long, T., Thirlwall, M., and Cuong, T. X. (2021). Ages and character of igneous rocks of the Da Lat Zone in SE Vietnam and adjacent offshore regions (Cuu Long and Nam Con Son basins), *Journal of Asian Earth Sciences*, *218*, doi:10487810.1016/j.jseaes.2021.104878.

Hibbard, M. J. (1987). Deformation of incompletely crystallized magma systems: Granitic gneisses and their tectonic implications, *Journal of Geology*, *95*(4), 543-561, doi:10.1086/629148.

Huang, C. H., and Lin, C. L. (2019). Zircon U-Pb age of the Lufengshan miarolitic granite in Fujian Province and its geological significance, *East China Geology*, *40*(3), 170-178.

Huang, F., and Lundstrom, C. C. (2007). Pa-231 excesses in arc volcanic rocks: Constraint on melting rates at convergent margins, *Geology*, *35*(11), 1007-1010, doi:10.1130/g23822a.1.

Hutchison, C. S., and Vijayan, V. R. (2010). What are the Spratly Islands?, *Journal of Asian Earth Sciences*, *39*(5), 371-385, doi:10.1016/j.jseaes.2010.04.013.

Jelinek, V. (1981). Characterization of the magnetic fabric of rocks, *Tectonophysics*, *79*(3-4), T63-T67, doi:10.1016/0040-1951(81)90110-4.

Ji, W.-Q., Wu, F.-Y., Chung, S.-L., Wang, X.-C., Liu, C.-Z., Li, Q.-L., Liu, Z.-C., Liu, X.-C., and Wang, J.-G. (2016). Eocene Neo-Tethyan slab breakoff constrained by 45 Ma oceanic island basalt-type magmatism in southern Tibet, *Geology*, *44*(4), 283-286, doi:10.1130/g37612.1.

Ji, W. B., Faure, M., Lin, W., Chen, Y., Chu, Y., and Xue, Z. H. (2018). Multiple Emplacement and Exhumation History of the Late Mesozoic Dayunshan-Mufushan Batholith in Southeast China and Its Tectonic Significance: 1. Structural Analysis and Geochronological Constraints, *J Geophys Res-Sol Ea*, *123*(1), 689-710, doi:10.1002/2017jb014597.

Jiang, X.-Y., Li, X.-H., Collins, W. J., and Huang, H.-Q. (2015). U-Pb age and Hf-O isotopes of detrital zircons from Hainan Island: Implications for Mesozoic subduction models, *Lithos*, *239*, 60-70, doi:10.1016/j.lithos.2015.10.006.

Kemp, A. I. S., Hawkesworth, C. J., Collins, W. J., Gray, C. M., Blevin, P. L., and Eimf (2009). Isotopic evidence for rapid continental growth in an extensional accretionary orogen: The Tasmanides, eastern Australia, *Earth and Planetary Science Letters*, *284*(3-4), 455-466, doi:10.1016/j.epsl.2009.05.011.

Kimura, G., Kitamura, Y., Yamaguchi, A., Kameda, J., Hashimoto, Y., and Hamahashi, M. (2019). Origin of the early Cenozoic belt boundary thrust and Izanagi-Pacific ridge subduction in the western Pacific margin, *Island Arc*, *28*(5), doi:e1232010.1111/iar.12320.

Knittel, U., Hung, C. H., Yang, T. F., and Iizuka, Y. (2010). Permian arc magmatism in Mindoro, the Philippines: An early Indosinian event in the Palawan Continental Terrane, *Tectonophysics*, *493*(1-2), 113-117, doi:10.1016/j.tecto.2010.07.007.

Kudrass, H. R., Wiedicke, M., Cepek, P., Kreuzer, H., and Müller, P. (1986). Mesozoic and Cainozoic rocks dredged from the South China Sea (Reed Bank area) and Sulu Sea and their significance for plate-tectonic reconstructions, *Marine and Petroleum Geology*, *3*, 19-30.

Li, J., Zhang, Y., Dong, S., and Johnston, S. T. (2014). Cretaceous tectonic evolution of South China: A preliminary synthesis, *Earth-Science Reviews*, *134*(0), 98-136, doi:http://dx.doi.org/10.1016/j.earscirev.2014.03.008.

Li, L. M., Sun, M., Xing, G. F., Zhao, G. C., Zhou, M. F., Wong, J., and Chen, R. (2009). Two late Mesozoic volcanic events in Fujian Province: constraints on the tectonic evolution of southeastern China, *Int Geol Rev*, *51*(3), 216-251, doi:Pii 90903773610.1080/00206810802619092.

Li, W. X., Zhou, X. M., and Li, X. H. (2003). U-Pb and 40Ar/ 39Ar dating of deformed igneous rocks from the Changle-Nan'ao fault, *Chinese Journal of Geology*, *38*(1), 22-30.

Li, X.-Y., Li, S.-Z., Suo, Y.-H., Dai, L.-M., Guo, L.-L., Ge, F.-J., and Lin, P.-J. (2018). Late Cretaceous basalts and rhyolites from Shimaoshan Group in eastern Fujian Province, SE China: age, petrogenesis, and tectonic implications, *Int Geol Rev*, *60*(11-14), 1721-1743, doi:10.1080/00206814.2017.1353447.

Li, Y., Ma, C.-Q., Xing, G.-F., and Zhou, H.-W. (2015). The Early Cretaceous evolution of SE China: Insights from the Changle-Nan'ao Metamorphic Belt, *Lithos*, *230*, 94-104, doi:10.1016/j.lithos.2015.05.014.

Li, Y. X., Ali, J. R., Chan, L. S., and Lee, C. M. (2005). New and revised set of Cretaceous paleomagnetic poles from Hong Kong: implications for the development of southeast China, *Journal of Asian Earth Sciences*, *24*(4), 481-493, doi:10.1016/j.jseaes.2004.01.004.

Li, Z., Wang, X.-C., Wilde, S. A., Liu, L., Li, W.-X., and Yang, X. (2018). Role of deep-Earth water cycling in the growth and evolution of continental crust: Constraints from Cretaceous magmatism in southeast China, *Lithos*, *302*, 126-141, doi:10.1016/j.lithos.2017.12.028.

Li, Z. X., and Li, X. H. (2007). Formation of the 1300-km-wide intracontinental orogen and postorogenic magmatic province in Mesozoic South China: A flat-slab subduction model, *Geology*, *35*(2), 179-182, doi:10.1130/g23193a.1.

Liang, Y., Delescluse, M., Qiu, Y., Pubellier, M., Chamot-Rooke, N., Wang, J., Nie, X., Watremez, L., Chang, S.-P., Pichot, T., Savva, D., and Meresse, F. (2019). Decollements, Detachments, and Rafts in the Extended Crust of Dangerous Ground, South China Sea: The Role of Inherited Contacts, *Tectonics*, *38*(6), 1863-1883, doi:10.1029/2018tc005418.

Lin, W., and Wei, W. (2018). Late Mesozoic extensional tectonics in the North China Craton and its adjacent regions: a review and synthesis, *Int Geol Rev*, 1-29.

Lin, W., Zeng, J., Meng, L., Qiu, H., Wei, W., Ren, Z., Chu, Y., Li, S., Song, C., and Wang, Q. (2021). Extensional tectonics and North China Craton destruction: Insights from the magnetic susceptibility anisotropy (AMS) of granite and metamorphic core complex, *Science China-Earth Sciences*, *64*(9), 1557-1589, doi:10.1007/s11430-020-9754-1.

Liu, Q., Yu, J. H., Su, B., Wang, Q., Tang, H. F., Xu, H., and Cui, X. (2011). Discovery of the 187Ma granite in Jincheng area, Fujian Province: Constraint on Early Jurassic tectonic evolution of southeastern China, *Acta Petrologica Sinica*, *27*(12), 3575-3589.

Liu, Q., Yu, J. H., Wang, Q., Su, B., Zhou, M. F., Xu, H., and Cui, X. (2012). Ages and geochemistry of granites in the Pingtan-Dongshan Metamorphic Belt, Coastal South China: New constraints on Late Mesozoic magmatic evolution, *Lithos*, *150*, 268-286, doi:10.1016/j.lithos.2012.06.031.

Ludwig, K. R. (2003). *User's Manual for Isoplot 3.0: a Geochronological Toolkit for Microsoft Excel. 4.*, 1 – 71 pp., Berkeley Geochronology Center Special Publication.

Lyra, D. S., Savian, J. F., Bitencourt, M. d. F., Trindade, R. I. F., and Tome, C. R. (2018). AMS fabrics and emplacement model of Buda Granite, an Ediacaran syntectonic peraluminous granite from southernmost Brazil, *Journal of South American Earth Sciences*, *87*, 25-41, doi:10.1016/j.jsames.2017.12.006.

Magni, V., Faccenna, C., van Hunen, J., and Funiciello, F. (2013). Delamination vs. break-off: the fate of continental collision, *Geophysical Research Letters*, *40*(2), 285-289, doi:10.1002/grl.50090.

Mattauer, M., Matte, P., Malavieille, J., Tapponnier, P., Maluski, H., Xu, Z. Q., Lu, Y. L., and Tang, Y. Q. (1985). Tectonics of the Qinling belt - buildup and evolution of eastern Asia, *Nature*, *317*(6037), 496-500, doi:10.1038/317496a0.

Morley, C. K. (2012). Late Cretaceous – Early Palaeogene tectonic development of SE Asia, *Earth-Science Reviews*, *115*(1 – 2), 37-75, doi:http://dx.doi.org/10.1016/j.earscirev.2012.08.002.

Nédélec, A., Bowden, P., and Bouchez, J. L. (2015). *GRANITES: Petrology, structure, geological setting, and metallogeny*, GRANITES: Petrology, structure, geological setting, and metallogeny.

Parrish, R. R. (1990). U-Pb dating of monazite and its application to geological problems, *Canadian Journal of Earth Sciences*, *27*(11), 1431-1450.

Passchier, C. W., and Trouw, R. (2005). *Microtectonics*, Springer Berlin Heidelberg, New York.

Paterson, S. R., and Ducea, M. N. (2015), Arc Magmatic Tempos: Gathering the Evidence, *Elements*, *11*(2), 91-97, doi:10.2113/gselements.11.2.91.

Paterson, S. R., Fowler, T. K., Schmidt, K. L., Yoshinobu, A. S., Yuan, E. S., and Miller, R. B. (1998). Interpreting magmatic fabric patterns in plutons, *Lithos*, *44*(1-2), 53-82, doi:10.1016/s0024-4937(98)00022-x.

Pitcher, W. S. (1979). The nature, ascent and emplacement of granitic magmas, *Journal of the Geological Society*, *136*(NOV), 627-662, doi:10.1144/gsjgs.136.6.0627.

Pommier, A., Cocherie, A., and Legendre, O. (2003). EPMA dating: a program for age calculation from electron microprobe measurements of U-Th-Pb, in *EGU2003*, edited.

Qiu, J. S., Wang, D. Z., and Zhou, J. C. (1999). Geochemistry and petrogenesis of the late mesozoic bimodal volcanic rocks at yunshan caldera, Yongtai country, Fujian province, *Acta Petrologica et Mineralogica*, *18*(2), 97-107.

Raposo, M. I. B., and Ernesto, M. (1995). Anisotropy of magnetic-susceptibility in the Ponta-Grossa dyke swarm (Brazil) and its relationship with magma flow direction, *Physics of the Earth and Planetary Interiors*, *87*(3-4), 183-196, doi:10.1016/0031-9201(94)02970-m.

Rochette, P., Jackson, M., and Aubourg, C. (1992). Rock magnetism and the interpretation of anisotropy of magnetic susceptibility, *Reviews of Geophysics*, *30*(3), 209-226, doi:10.1029/92rg00733.

Roman-Berdiel, T., Aranguren, A., Cuevas, J., and Tubia, J. M. (1998). Compressional granite-emplacement model: structural and magnetic study of the Trives Massif (NW Spain), *Lithos*, *44*(1-2), 37-52.

Rubatto, D. (2002). Zircon trace element geochemistry: partitioning with garnet and the link between U-Pb ages and metamorphism, *Chemical Geology*, *184*(1-2), 123-138, doi:Pii s0009-2541(01)00355-210.1016/s0009-2541(01)00355-2.

Sagong, H., Kwon, S. T., and Ree, J. H. (2005). Mesozoic episodic magmatism in South Korea and its tectonic implication, *Tectonics*, *24*(5), doi:Tc500210.1029/2004tc001720.

Sen, K., Majumder, S., and Mamtani, M. A. (2005). Degree of magnetic anisotropy as a strain intensity gauge in ferromagnetic granites, *Journal of the Geological Society*, *162*, 583-586, doi:10.1144/0016-764904-144.

Shellnutt, J. G., Lee, T.-Y., Brookfield, M. E., and Chung, S.-L. (2014). Correlation between magmatism of the Ladakh Batholith and plate convergence rates during the India-Eurasia collision, *Gondwana Research*, *26*(3-4), 1051-1059, doi:10.1016/j.gr.2013.09.006.

Shu, L., Yao, J., Wang, B., Faure, M., Charvet, J., and Chen, Y. (2021). Neoproterozoic plate tectonic process and Phanerozoic geodynamic evolution of the South China Block, *Earth-Science Reviews*, *216*, doi:10359610.1016/j.earscirev.2021.103596.

Shu, L. S., Zhou, X. M., Deng, P., Wang, B., Jiang, S. Y., Yu, J. H., and Zhao, X. X. (2009). Mesozoic tectonic evolution of the Southeast China Block: New insights from basin analysis, *Journal of Asian Earth Sciences*, *34*(3), 376-391, doi:10.1016/j.jseaes.2008.06.004.

Simpson, C., and Wintsch, R. P. (1989). Evidence for deformation-induced K-feldspar replacement by myrmekite, *Journal of Metamorphic Geology*, *7*(2), 261-275.

Suggate, S. M., Cottam, M. A., Hall, R., Sevastjanova, I., Forster, M. A., White, L. T., Armstrong, R. A., Carter, A., and Mojares, E. (2014). South China continental margin signature for sandstones and granites from Palawan, Philippines, *Gondwana Research*, *26*(2), 699-718, doi:10.1016/j.gr.2013.07.006.

Tarling, D. H., and Hrouda, F. (1993). *The magnetic anisotropy of rocks*, 1-217 pp., Chapman & Hall, London.

Tong, W. X., and Tobisch, O. T. (1996). Deformation of granitoid plutons in the Dongshan area, southeast China: Constraints on the physical conditions and timing of movement along the Changle-Nanao shear zone, *Tectonophysics*, *267*(1-4), 303-316.

Tripathy, N. R. (2009). Degree of magnetic anisotropy as a strain-intensity gauge in a saturated finite-strain zone, *Journal of the Geological Society*, *166*, 9-12, doi:10.1144/0016-76492008-078.

Turrillot, P., Faure, M., Martelet, G., Chen, Y., and Augier, R. (2011). Pluton-dyke relationships in a Variscan granitic complex from AMS and gravity modelling. Inception of the extensional tectonics in the South Armorican Domain (France), *Journal of Structural Geology*, *33*(11), 1681-1698, doi:10.1016/j.jsg.2011.08.004.

Van Hunen, J., and Allen, M. B. (2011). Continental collision and slab break-off: A comparison of 3-D numerical models with observations, *Earth and Planetary Science Letters*, *302*(1-2), 27-37, doi:10.1016/j.epsl.2010.11.035.

Vermeesch, P. (2018). IsoplotR: A free and open toolbox for geochronology, *Geoscience Frontiers*, *9*(5), 1479-1493, doi:10.1016/j.gsf.2018.04.001.

Vernon, R. H. (2000). Review of Microstructural Evidence of Magmatic and Solid-State Flow, *Electronic Geosciences*, *5*(2).

Wang, Z. H., and Lu, H. F. (1997). Evidence and dynamics for the change of strike-slip direction of the Changle-Nanao ductile shear zone, southeastern China, *Journal of Asian Earth Sciences*, *15*(6), 507-515.

Wang, Z. H., and Lu, H. F. (2000). Ductile deformation and Ar-40/Ar-39 dating of the Changle-Nanao ductile shear zone, southeastern China, *J Struct Geol*, *22*(5), 561-570, doi:10.1016/s0191-8141(99)00179-0.

Wei, W., Chen, Y., Faure, M., Martelet, G., Lin, W., Wang, Q., Yan, Q., and Hou, Q. (2016). An early extensional event of the South China Block during the Late Mesozoic recorded by the emplacement of the Late Jurassic syntectonic Hengshan Composite Granitic Massif (Hunan, SE China), *Tectonophysics*, *672–673*, 50-67, doi:http://dx.doi.org/10.1016/j.tecto.2016.01.028.

Wei, W., Chen, Y., Faure, M., Shi, Y. H., Martelet, G., Hou, Q. L., Lin, W., Le Breton, N., and Wang, Q. C. (2014). A multidisciplinary study on the emplacement mechanism of the Qingyang–Jiuhua Massif in Southeast China and its tectonic bearings. Part I: Structural geology, AMS and paleomagnetism, *Journal of Asian Earth Sciences*, *86*(0), 76-93, doi:http://dx.doi.org/10.1016/j.jseaes.2013.06.003.

Wei, W., Faure, M., Chen, Y., Ji, W., Lin, W., Wang, Q., Yan, Q., and Hou, Q. (2015). Back-thrusting response of continental collision: Early Cretaceous NW-directed thrusting in the Changle-Nan'ao belt (Southeast China), *Journal of Asian Earth Sciences*, *100*, 98-114.

Wei, W., Song, C., Hou, Q., Chen, Y., Faure, M., Yan, Q., Liu, Q., Sun, J., and Zhu, H. (2018). The Late Jurassic extensional event in the central part of the South China Block – evidence from the Laoshan'ao shear zone and Xiangdong Tungsten deposit (Hunan, SE China), *Int Geol Rev*, 1-21, doi:10.1080/00206814.2017.1395714.

Wu, F.-Y., Han, R.-H., Yang, J.-H., Wilde, S. A., Zhai, M.-G., and Park, S.-C. (2007). Initial constraints on the timing of granitic magmatism in North Korea using U-Pb zircon geochronology, *Chemical Geology*, *238*(3-4), 232-248, doi:10.1016/j.chemgeo.2006.11.012.

Wu, F.-Y., Yang, J.-H., Xu, Y.-G., Wilde, S. A., and Walker, R. J. (2019). Destruction of the North China Craton in the Mesozoic, in *Annual Review of Earth and Planetary Sciences, Vol 47*, edited by Jeanloz, R. and Freeman, K. H., pp. 173-195, doi:10.1146/annurev-earth-053018-060342.

Wu, F.-Y., Yang, Y.-H., Xie, L.-W., Yang, J.-H., and Xu, P. (2006). Hf isotopic compositions of the standard zircons and baddeleyites used in U-Pb geochronology, *Chemical Geology*, *234*(1-2), 105-126, doi:10.1016/j.chemgeo.2006.05.003.

Xie, L., Zhang, Y., Zhang, H., Sun, J., and Wu, F. (2008). In situ simultaneous determination of trace elements, U-Pb and Lu-Hf isotopes in zircon and baddeleyite, *Chinese Science Bulletin*, *53*(10), 1565-1573, doi:10.1007/s11434-008-0086-y.

Xu, J., Zhu, G., Tong, W., Cui, K., and Liu, Q. (1987). Formation and evolution of the Tancheng-Lujiang wrench fault system: a major shear system to the northwest of the Pacific Ocean, *Tectonophysics*, *134*(4), 273-310.

Xu, X. B. (2019). Magma mixing and tectonic significance of Dongzhuang intrusion in the middle section of the Changle-Nan'ao structure zone *Geology of Fujian*, *038*(004), 248-262.

Yan, P., and Liu, H. L. (2004). Tectonic-stratigraphic division and blind fold structures in Nansha Waters, South China Sea, *Journal of Asian Earth Sciences*, *24*(3), 337-348, doi:10.1016/j.jseaes.2003.12.005.

Yao, B., Li, Z., Wei, Z., Hai, Y., and Li, C. (2011). The Mesozoic tectonic characteristics and sedimentary basins in the eastern margin of South China, *Marine Geology & Quaternary Geology*, *31*(3), 47-60.

Yumul, G. P., Jr. (2007). Westward younging disposition of Philippine ophiolites and its implication for arc evolution, *Island Arc*, *16*(2), 306-317, doi:10.1111/j.1440-1738.2007.00573.x.

Yumul Jr, G. P., Dimalanta, C. B., Marquez, E. J., and Queaño, K. L. (2009). Onland signatures of the Palawan microcontinental block and Philippine mobile belt collision and crustal growth process: A review, *Journal of Asian Earth Sciences*, *34*(5), 610-623, doi:http://dx.doi.org/10.1016/j.jseaes.2008.10.002.

Zak, J., Dragoun, F., Verner, K., Chlupacova, M., Holub, F. V., and Kachlik, V. (2009). Forearc deformation and strain partitioning during growth of a continental magmatic arc: The northwestern margin of the Central Bohemian Plutonic Complex, Bohemian Massif, *Tectonophysics*, *469*(1-4), 93-111, doi:10.1016/j.tecto.2009.01.035.

Zak, J., Schulmann, K., and Hrouda, F. (2005). Multiple magmatic fabrics in the Sazava pluton (Bohemian Massif, Czech Republic): a result of superposition of wrench-dominated regional transpression on final emplacement, *Journal of Structural Geology*, *27*(5), 805-822, doi:10.1016/j.jsg.2005.01.012.

Zamoras, L. R., and Matsuoka, A. (2004). Accretion and postaccretion tectonics of the Calamian Islands, North Palawan block, Philippines, *Island Arc*, *13*(4), 506-519, doi:10.1111/j.1440-1738.2004.00443.x.

Zhang, S., Zhang, X., Zhang, Q., and She, Q. (2015). Characteristics of the Cretaceous in the Northern South China Sea and tectonic implications, *Marine Geology & Quaternary Geology*.

Zhang, X., Chung, S.-L., Lai, Y.-M., Ghani, A. A., Murtadha, S., Lee, H.-Y., and Hsu, C.-C. (2019). A 6000-km-long Neo-Tethyan arc system with coherent magmatic flare-ups and lulls in South Asia, *Geology*, *47*(6), 573-576, doi:10.1130/g46172.1.

Zhao, J.-L., Qiu, J.-S., Liu, L., and Wang, R.-Q. (2015). Geochronological, geochemical and Nd-Hf isotopic constraints on the petrogenesis of Late Cretaceous A-type granites from the southeastern coast of Fujian Province, South China, *Journal of Asian Earth Sciences*, *105*, 338-359, doi:10.1016/j.jseaes.2015.01.022.

Zhao, J.-L., Qiu, J.-S., Liu, L., and Wang, R.-Q. (2016). The Late Cretaceous I- and A-type granite association of southeast China: Implications for the origin and evolution of post-collisional extensional magmatism, *Lithos*, *240*, 16-33, doi:10.1016/j.lithos.2015.10.018.

Zhou, D., Sun, Z., Chen, H. Z., Xu, H. H., Wang, W. Y., Pang, X., Cai, D. S., and Hu, D. K. (2008). Mesozoic paleogeography and tectonic evolution of South China Sea and adjacent areas in the context of Tethyan and Paleo-Pacific interconnections, *Island Arc*, *17*(2), 186-207, doi:10.1111/j.1440-1738.2008.00611.x.

Zhou, L., Wang, Y., Hei, H., and Zhou, X. (2016). Early Cretaceous Magma Mingling in Xiaocuo, Southeastern China Continental Margin: Implications for Subduction of Paleo-Pacific Plate, *Acta Geologica Sinica-English Edition*, *90*(5), 1713-1742, doi:10.1111/1755-6724.12812.

Zhou, X. M., Sun, T., Shen, W. Z., Shu, L. S., and Niu, Y. L. (2006). Petrogenesis of Mesozoic granitoids and volcanic rocks in South China: A response to tectonic evolution, *Episodes*, *29*(1), 26-33.

Zhu, R., Liu, H., Yao, Y., and Wang, Y. (2018). Mesozoic Deformation and Its Geological Significance in the Southern Margin of the South China Sea, *Journal of Ocean University of China*, *17*(4), 835-845, doi:10.1007/s11802-018-3581-z.

Figure captions

Figure 1. The schematic tectonic map of the East Asia Continental Margin. (a) South China block and Dangerous Grounds-West Philippine microcontinental Block; the compression direction and shortening ratio are after Zhu et al., 2018; (b) the igneous age distribution of the NCC (Wu et al., 2019); (c) the igneous age distribution of the SCB (Jiang et al., 2015); (d) suture zone between the South China Block and the Dangerous Grounds-West Philippines microcontinental Block recorded in the West Philippines islands; the geologic map was modified after Faure and Ishida, 1990; Zamoras and Matsuoka, 2004.

Figure 2. The simplified geologic map and geochronologic data of the Changle-Nan'ao belt (CNB). (a) the structural map; b, the age distribution of zircons of volcanic rocks in the CNB, modified after Guo et al., 2012; (b) and (c) Age distribution of plutons in the CNB, the data and citations of previous chronological studies refer to Appendix Table S1; (e)-(h) visible fabrics of different lithologies in the CNB (modified after Wei et al., 2015), the A-type lineation will clustered in the shaded area (NW-SE direction) in (g) and (h) after correction of foliation to flat, details refer to Wei et al., 2015; K_2sh: Upper Cretaceous undeformed volcanic rocks of the Shimaoshan Formation; K_1n: the Lower Cretaceous deformed volcanic rocks of the Nanyuan Formation; J_3dl: the Upper Jurassic deformed volcanic rocks of the Douling Formation.

Figure 3. Field observations on the plutons and their country rocks in the CNB. (a) magmatic foliation defined by the biotite and feldspars preferred orientation in the Dongzhuang granodiorite (refer to FJ05 in Fig. 6 for the location). (b) microgranite mafic enclaves in the Gaoshan pluton (refer to FJ54 in Fig. 6 for the location), the orientation of the enclaves is NE-striking with steep inclination to the NW and parallel with magmatic foliation as well as the host granite. (c) microgranitoid enclaves and schlierens in the Hui'an pluton (refer to FJ55 in Fig. 6 for the location). The enclaves developed tails or even evolved into schlieren indicating that the convection of the host Hui'an granite was still active during the intrusion of the mafic melts. (d) granitic dyke of the Matui stock intruded into the Early Cretaceous deformed volcanic rocks (refer to FJ53 in Fig. 6 for the location), the contact boundary is wavy, and the magmatic foliation is parallel to the boundary and the foliation of the deformed volcanic rocks. (e) xenolith of deformed volcanic rocks in the granite of Matui stock (refer to FJ53 in Fig. 6 for the location), the boundary of the xenolith is wavy and the magmatic foliation of the granite surrounds the xenolith. (f) ductile deformation of the boundary of the Hui'an pluton (refer to FJ65 in Fig. 6 for the location). (g) the isotropic structure of the core of the Hui'an pluton (refer to FJ62 in Fig. 6 for the location). (h) Country rock (hornfels sandstone) of the Hui'an pluton, showing contact metamorphism (refer to FJ59 in Fig. 6 for the location).

Figure 4. magnetic characters of syn-tectonic granitoids in CNB. (a) Histogram of bulk magnetic susceptibility, N=39. (b) Day-Plot diagram to define the magnetite size, Mrs: remanence, Ms: saturation remanence, Hcr: coercivity of remanence, Hc: coercivity, SD: single domain, PSD: pseu-single domain, MD: multi-domain, respectively. (c) P_J (corrected anisotropy degree) vs. Km (mean bulk magnetic susceptibility) , (d) T (shape parameter) vs. P_J. The calculation formulas of T and P_J can be found in Jelinek (1981).

Figure 5. Representative thermal-Susceptibility, hysteresis loop diagrams, Isothermal Remanent Magnetization (IRM) of CNB granitoids.

Figure 6. Equal-area lower hemisphere projection of AMS results of each site and whole individual plutons in the CNB. Squares and circles stand for K_1 (magnetic

lineation) and K_3 (pole of magnetic foliation), respectively. Small and large squares or circles represent individual specimen and site-mean direction with their confidence ellipses at 95% level, respectively. The yellow great circle in the stereo-projection represents the magmatic foliation measured in field.

Figure 7. Representative microscopic features of the plutons with oriented minerals in the CNB.
(a) In the Su'ao pluton (refer to FJ52 in Fig. 6 for the location), the biotite and feldspar were oriented along the magnetic foliation, myrmekite developed along the feldspar boundary which is parallel with the magnetic foliation, the boundary of quartz is suture shaped indicating a Grain Boundary Migration recovery. (b) In the granodiorite of the Dongzhuang Pluton (refer to FJ08 in Fig. 6 for the location), the amphibole and plagioclase were oriented along the vertical magnetic foliation, the plagioclase developed pressure shadow made by biotite in which the tiny quartz grain inclusions were present, the boundary between grains of feldspars and quartz were featured by suture shape. (c) in the Hui'an pluton (location refer to FJ57 in Fig. 6 for the location), quartz developed chessboard structure, the feldspar were cracked. (d) In the Damaoshan pluton (refer to FJ46 in Fig. 6), the feldspar is oriented along the vertical magnetic foliation, the feldspars were cracked and infilled with muscovite and quartz, the grain boundary between feldspars and between quartz were in suture shape, the biotite was bend. (e) In the diorite of the Tong'an pluton (refer to FJ24 in Fig. 6 for the location), the amphibole, biotite and feldspar were oriented along the vertical magnetic foliation, the feldspars were cracked and infilled with quartz, the boundary between grains of feldspars and quartz were in suture shape. (f) In the Longshoushan stock (refer to FJ84 in Fig. 6 for the location), the quartz and feldspar were oriented along the magnetic foliation, the quartz developed chessboard structure, the grain boundary between quartz was in suture shape. (g) Along the NE-SW horizontal thin section of the Longshoushan stock (refer to FJ84 in Fig. 6 for the location), the feldspar was oriented along the NE-SW striking mangetic foliation, the grain boudnary between feldspar, between quartz, and between quartz and feldspar were in suture shape. (h) In the Duxun pluton (location 13 in Fig. 2), the quartz grains show rectangular shape.

Figure 8. Zircon U-Pb isotropic dating (a-d) and Monazite U-Th-Pb chemical dating (e) results of the syn-tectonic granitoids in the CNB.

Figure 9. Zircon Hf isotropic statistics from different lithologies of the CNB and its adjacent area. (a) data from coastal Fujian area (an area locating to the east of the dashed rectangle marked by Fig. 9b in Fig. 1a, among these data, most are from CNB as marked by the yellow solid rectangle in Fig. 1a); (b) data form the interior Fujian area (location refer to the dashed rectangle marked by Fig. 9b in Fig. 1a).

Figure 10. A possible evolution model for the EACM during the Cretaceous. (a) In

the stage 1, the subduction of the Paleo-Pacific Slab led to a back-arc extension in the SCB and the magmatism in the Changle-Nan'ao belt while the DGWP Block carried by the Paleo-Pacific Slab was closing to the SCB; (b) In the stage 2, the DGWP Block collided with the SCB, leading to the development of fold and thrust belt of the CNB, the magmatic lull in the whole SCB, while the the slab window opened by the collision caused break-off of the subducted slab, led to the athenosphere upwelling and emplacement of syn-tectonic plutons with positive Hf isotropic feature in the CNB, owing to the shortening regime, the volcanic eruption ceased in the CNB; (3) In the stage 3, the newly formed subduction on the rear of the DGWP Block led to a back-arc extension in the SCB, and the post-orogenic magmatism in the CNB.

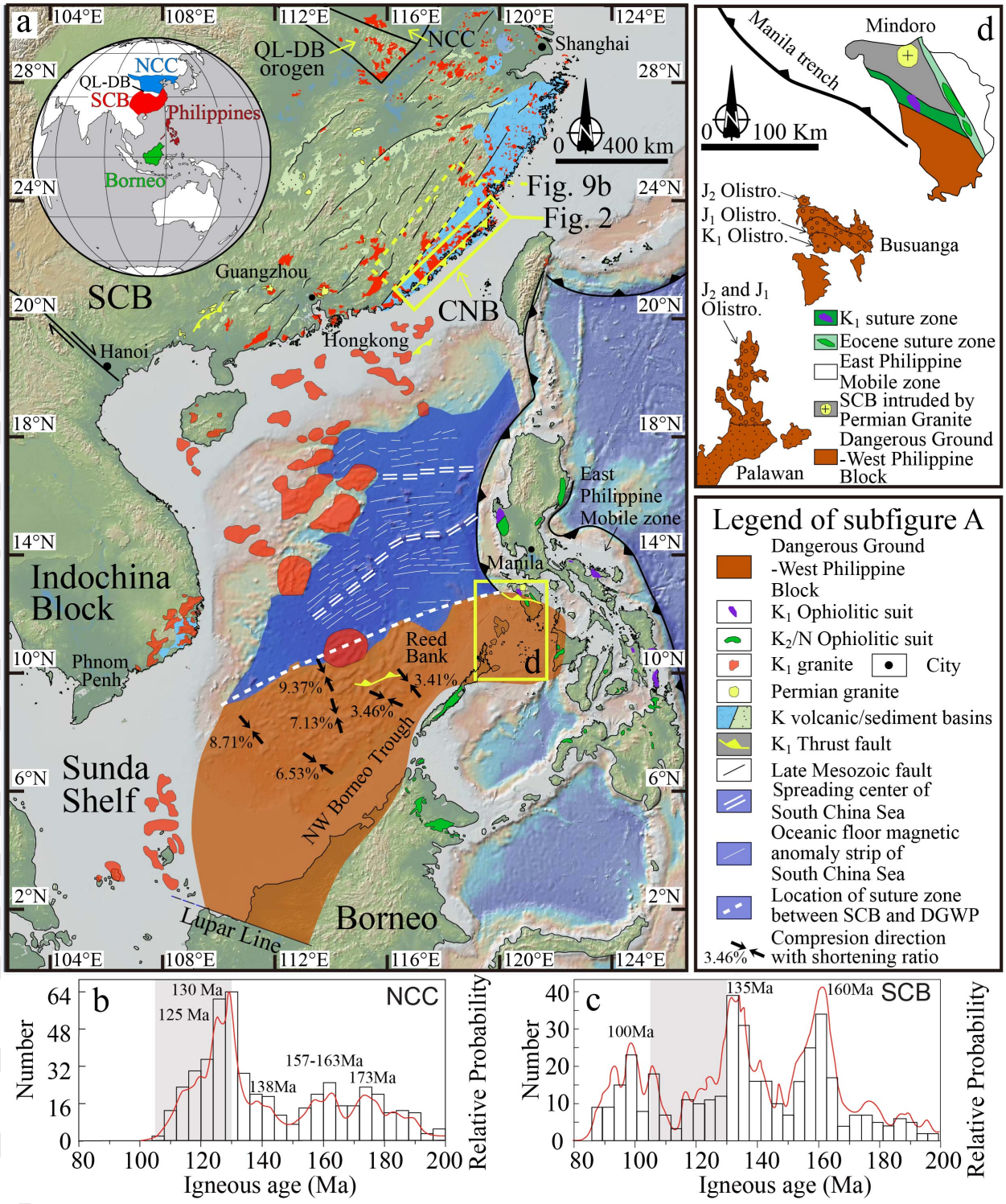

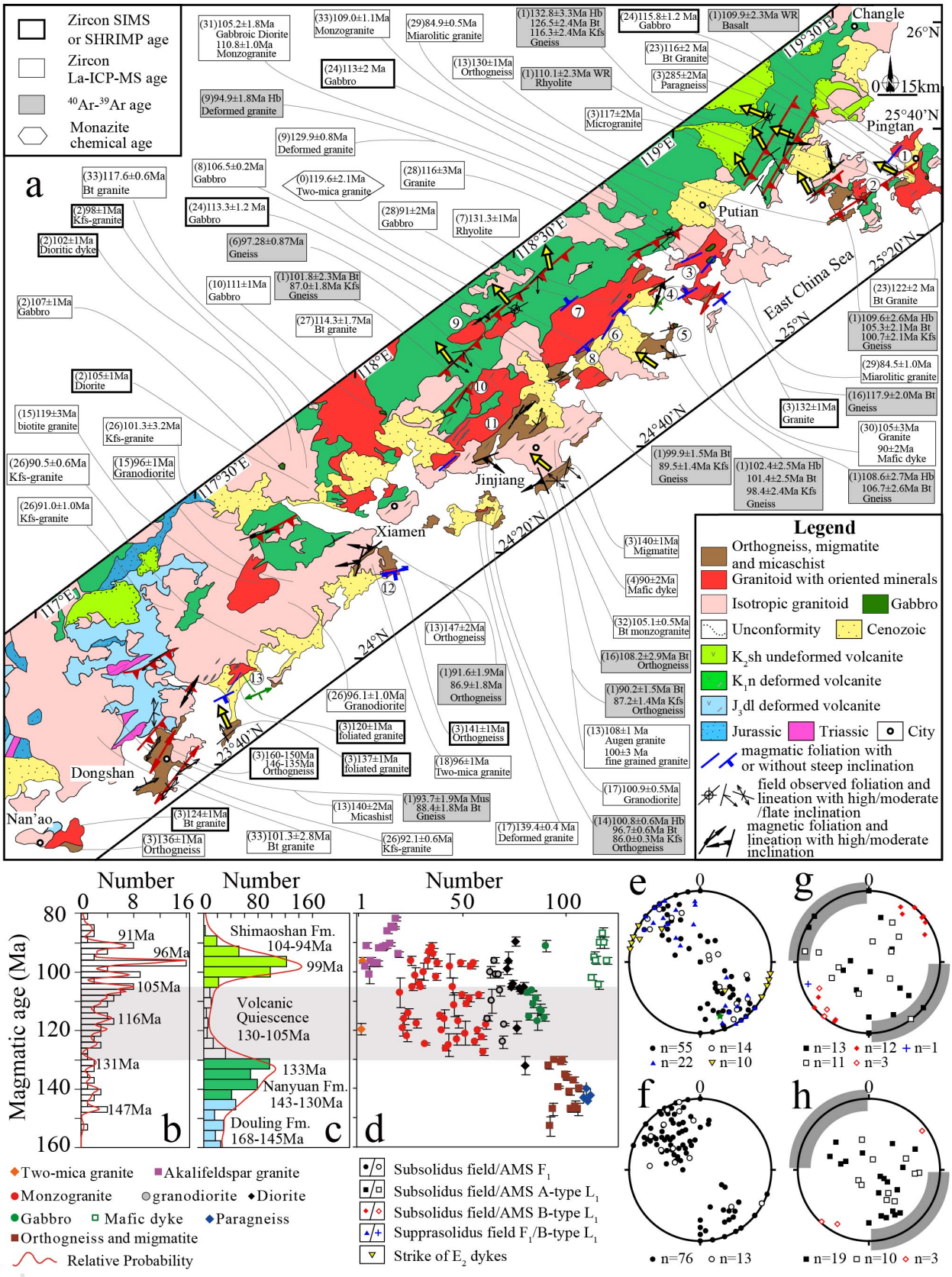

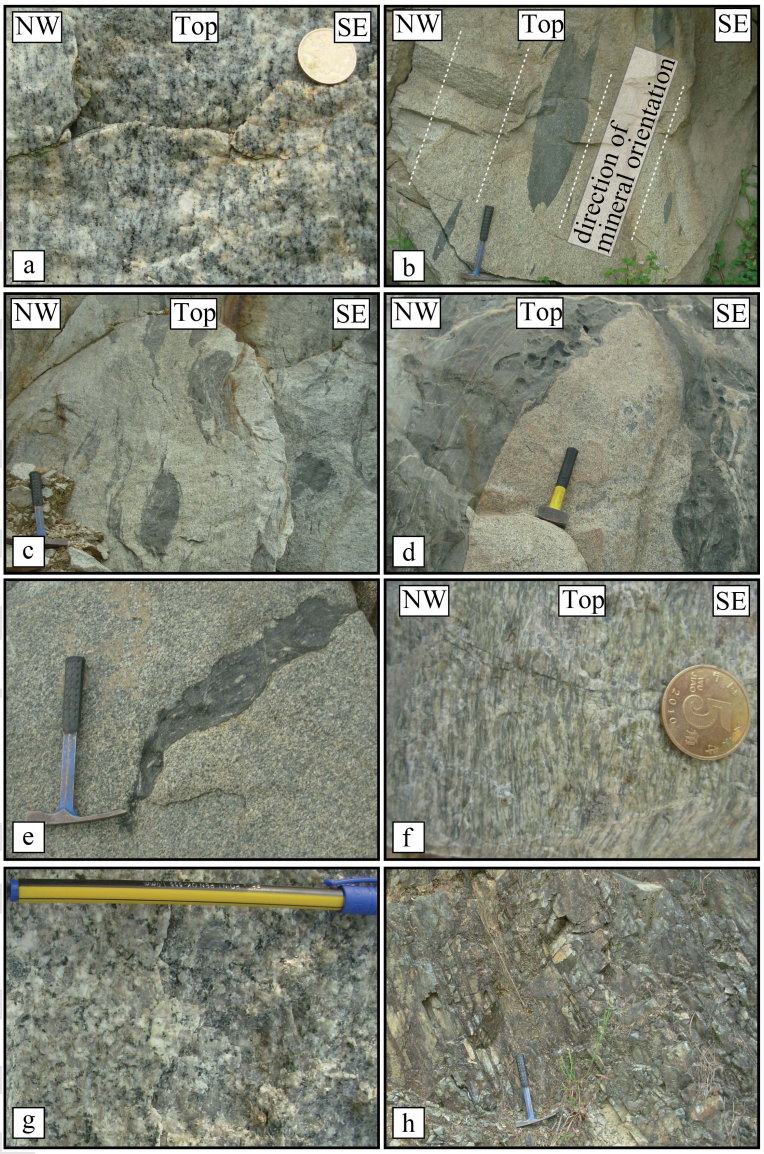

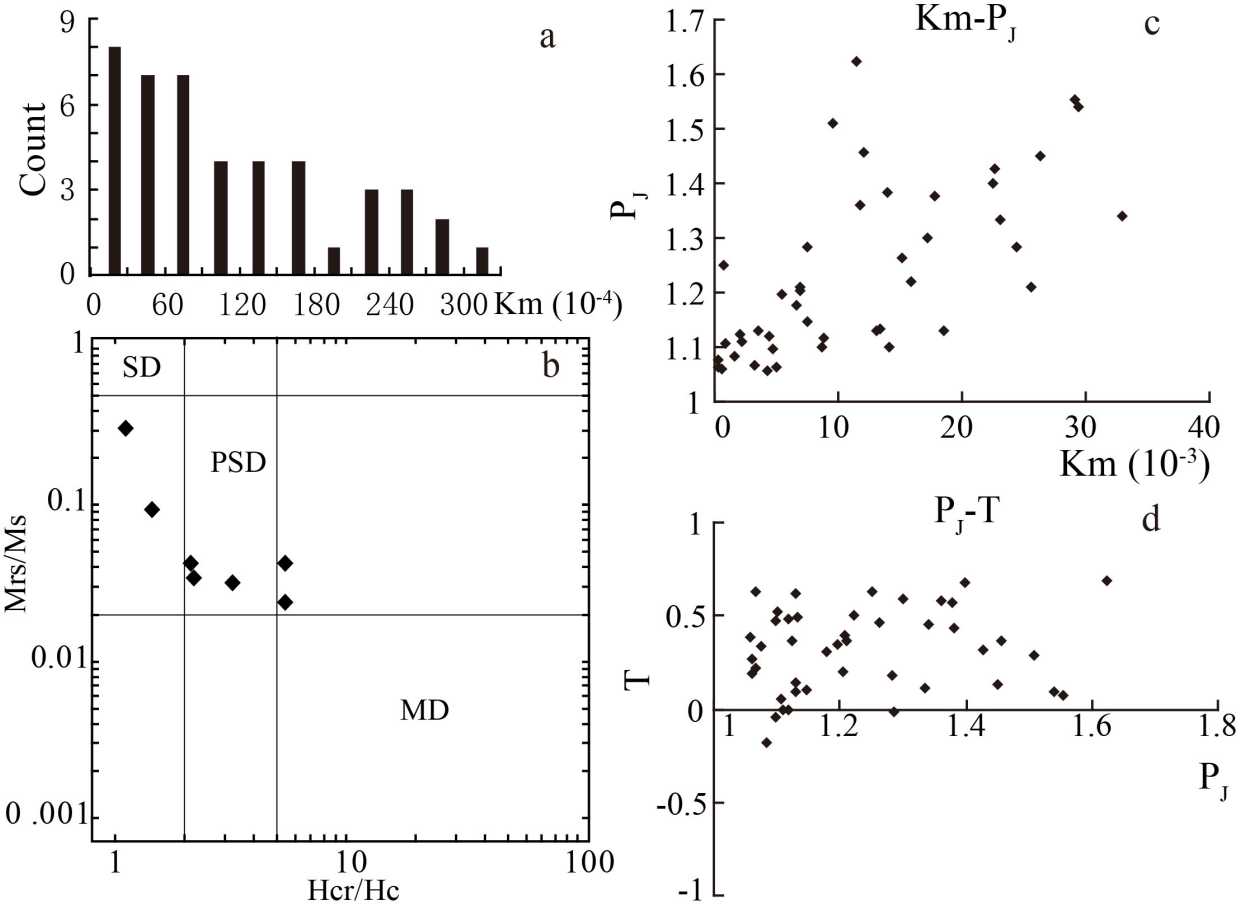

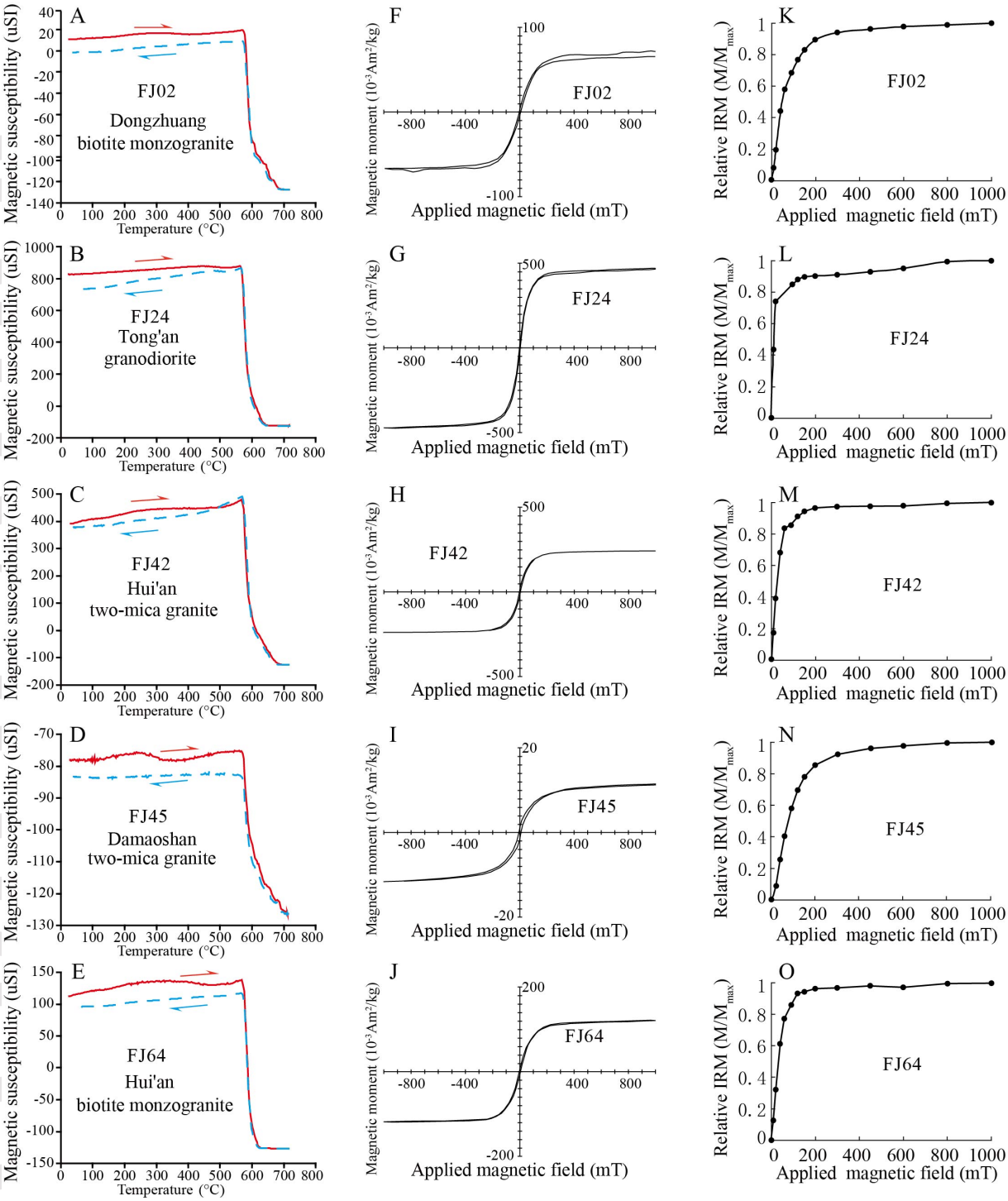

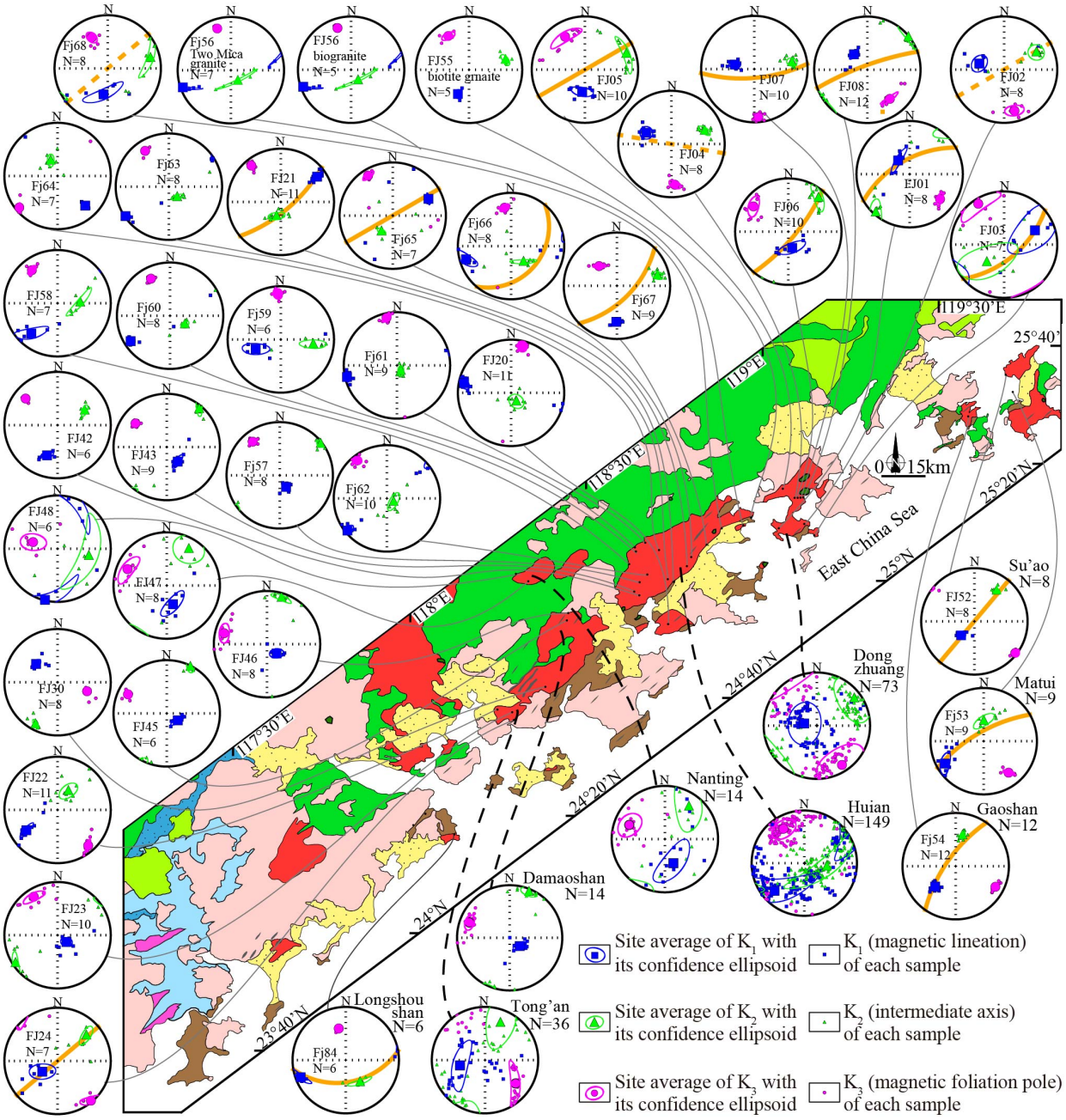

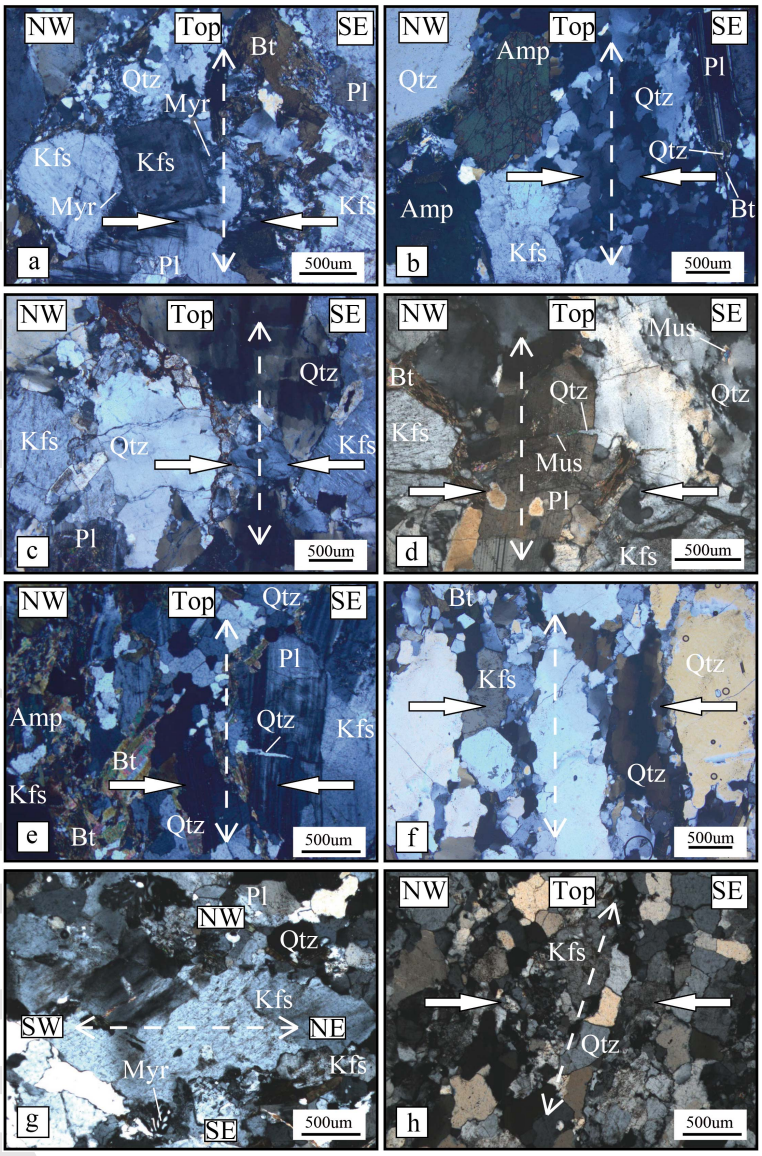

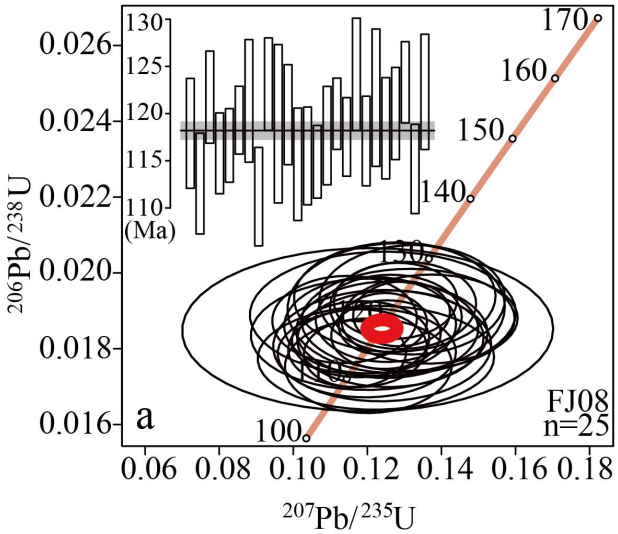

Concordia age = 118.38±0.57 MSWD=0.032
Mean age = 118.20±0.50 MSWD=1.76

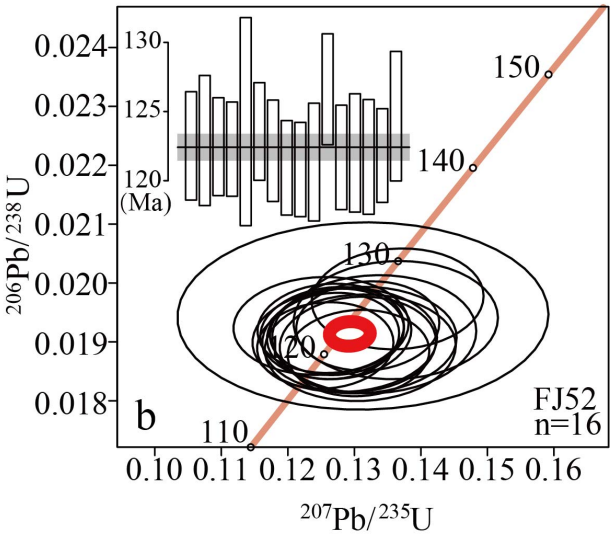

Concordia age = 122.41±0.50 MSWD=1.1
Mean age = 122.41±0.50 MSWD=0.53

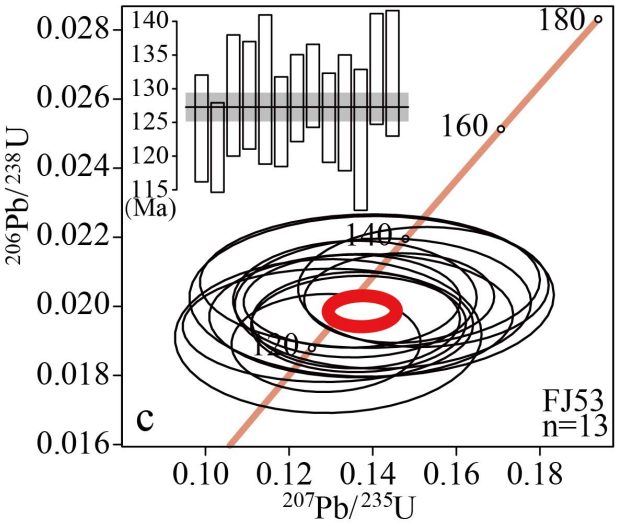

Concordia age = 127.27±1.09 MSWD=1.6
Mean age = 127.27±1.09 MSWD=0.82

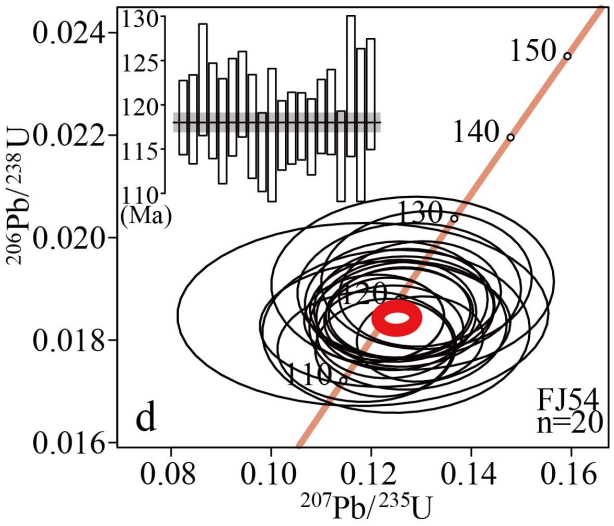

Concordia age = 118.00±1.57 MSWD=1.8
Mean age = 118.01±1.57 MSWD=0.68

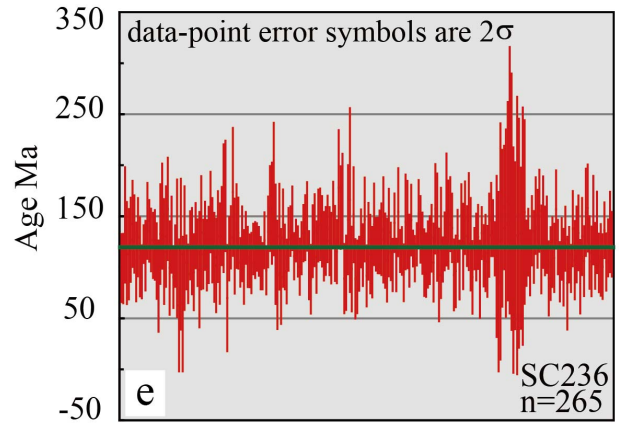

Mean age = 119.6±2.1 MSWD = 1.07